

표지

| (뒷면) | (측면) | (앞면) |
|---|--|--|
| <p>↑ 7cm ↓</p> <p>주 의 (편집 순서8) (16 포인트 코딕체)</p> | <p>빅토리아빙하코어시료의강설량복원을통한과거대기대순환복원</p> <p>이화여자대학교 ↑ 5cm ↓</p> | <p>↑ 7cm ↓</p> <p>빅토리아 빙하코어시료의 강설량복원을 통한 과거대기대순환 복원 (20 포인트 중고딕체)</p> <p>Reconstruction of past large-scale atmospheric circulation by reconstruction of snow accumulation rate from ice cores in Victoria land (16 포인트 명조체)</p> <p>이화여자대학교 (20 포인트 중고딕체)</p> <p>↓ 7cm ↑</p> |

제 출 문

극지연구소장 귀하

본 보고서를 “ 국제심부빙하시추 네트워크를 활용한 대기-빙상 상호작용의 자연적·인위적 특성규명” 과제의 위탁연구 “빅토리아랜드 빙하코어시료의 강설량복원을 통한 과거대기대순환 복원” 과제의 단계보고서로 제출합니다.



| | | |
|---------------|---|---------|
| (본과제) 총괄연구책임자 | : | 한영철 |
| 위탁연구기관명 | : | 이화여자대학교 |
| 위탁연구책임자 | : | 이정훈 |
| 위탁참여연구원 | : | 정혜정 |
| “ | : | 니암게렐알랄트 |
| “ | : | 강주리 |

보고서 초록

| | | | | | |
|--|-------------------------------------|--|------------|-------------|-------------|
| 위탁연구과제명 | 빅토리아랜드 빙하코어시료의 강설량복원을 통한 과거대기대순환 복원 | | | | |
| 위탁연구책임자 | 이정훈 | 해당단계 참여연구원수 | 4명 | 해당단계 연구비 | 180,000,000 |
| 연구기관명 및 소속부서명 | 이화여자대학교 과학교육과 지구과학전공 | | 참여기업명 | | |
| 국제공동연구 | 상대국명 : | | 상대국연구기관명 : | | |
| 요약(연구결과를 중심으로 개조식 500자이내) | | | | 보고서 면수 | |
| <p>본 연구는 남극 장보고기지 주변 빅토리아지역에서 국내 기술진으로 최초로 획득한 빙하시료를 이용하여 이 지역의 강설량을 복원하고 이를 통해 과거 기후인자를 찾고자 하는 것이 연구목적임. 이를 위해 스노우핏과 천부빙하코어 시료의 물안정동위원소를 측정하고 이를 바탕으로 연대측정을 시도하였음. 추정된 연대측정을 바탕으로 빅토리아지역의 강설량을 추정하였으며, 이를 통해 해빙과의 상관성을 추정하였음. 최근 해빙의 면적은 증가하고 있으며, 이에 강설량이 계속 줄어 드는 경향을 빅토리아 지역에서는 보여 주었음. 또한, 17O를 이용하여 과거 연구지역 주변의 습도를 추정하기 위한 연구에 대한 가능성을 제시하였음. 회토류원소에 대한 문헌조사를 통해 빙하연구 가능성을 제시하였음. 강설량과 함께 미량원소가 이러한 대기순환에 어떠한 영향을 받고 이러한 미량원소가 과거 대기순환의 프록시가 될 수 있을 지에 대한 연구를 수행하였음. 아문젠 해역등 해안지역 주변에서 천부빙하시료를 활용할 가능성을 대비하여 아문젠 해역 주변에서 획득한 스노우핏을 이용하여 연구지역의 강설량이 매우 높음을 제시하였음</p> | | | | | |
| 색 인 어 (각 5개 이상) | 한 글 | 빅토리아지역, 물동위원소, 과거대기대순환, 강설량, 아이스코어 | | | |
| | 영 어 | Victoria Land, Stable water isotopes, past atmospheric large scale circulation, ice core | | | |

요 약 문

I. 제 목

빅토리아랜드 빙하코어시료의 강설량복원을 통한 과거대기대순환 복원

II. 연구개발의 목적 및 필요성

본 연구에서는 빙하코어시료를 이용하여 남극 빅토리아랜드 주변의 고기후변화를 복원할 수 있는 방법을 제시하고 실제 극지연구소에서 보유하고 있는 다수의 빙하코어시료(4개)의 불안정동위원소 및 미량원소를 분석하여 과거대기대순환을 복원할 수 있는 기법을 연구하고자 함

III. 연구개발의 내용 및 범위

빙하시료를 이용한 남극 빅토리아 주변 강설량 복원 및 과거 기후인자와의 상관성을 통한 과거 대기대순환 복원

- 천부빙하코어의 불안정동위원소를 이용한 연대측정
- 연대측정을 통한 빅토리아랜드 강설량 복원
- 강설량, 미량원소와 기후인자간의 상관성 파악
- 이러한 기후인자와 빅토리아랜드 주변의 대기대순환(SAM, ASL)등과의 상관성확보
- 빙하코어시료를 이용하여 과거 대기대순환 복원

IV. 연구개발결과

스틱스지역의 편(firm) 코어의 불안정동위원소분석을 완료하였으며, 현재 미량원소분석을 수행하였음

- 스틱스빙하시료의 안정동위원소 및 주요이온, 모델결과를 활용하여 25년의 연대를 추정하였음
- 빙하의 연대측정을 통한 스틱스지역의 강설량을 추정하여 해빙과의 상관관계를 밝혔음
- 스노우핏 시료를 이용하여 해빙의 면적과 안정동위원소 값에 상관성이 있음을 밝혔음
- ^{17}O 의 빙하연구 가능성에 대하여 타진하였음
- 스노우핏을 이용하여 월평균안정동위원소 값이 대기온도와 상관관계가 있음을 밝혔음
- 빙하코어의 미량원소분석 결과를 향후 기상자료와 비교하기 위하여 스틱스지역에서 가져온 편코어의 미량원소 분석결과 분석 수행하고 있음
- 빙하코어의 melting layer 해석하기 위해 얼음 용해 실험 수행하였음

V. 연구개발결과의 활용계획

- 빙하 또는 편코어의 연대측정을 통한 강설량 복원기법은 향후 빙하시료분석의 원천기술로

- 활용될 것으로 기대됨
- 복원된 강설량은 극지역 기후변화의 프록시로 활용될 수 있음



S U M M A R Y

(영 문 요 약 문)

I. Title

Reconstruction of past large-scale atmospheric circulation by reconstruction of snow accumulation rate from ice cores in Victoria land

II. Purpose and Necessity of R&D

The scope of this research is related to the approach to reconstruct the past climate changes in regions near Victoria Land, Antarctica based on the ice core records, and the technique to reconstruct the large-scale climate circulation by analysing the water stable isotopes and trace elements in the ice cores obtained by Korea Polar Research Institute

III. Contents and Extent of R&D

Reconstruction of past large-scale atmospheric circulation in Victoria Land based on the relationship between snow accumulation rate reconstructed from ice core and past climate factors

- Age dating of shallow ice core based on water stable isotopes
- Estimation of snow accumulation rate based on the age scale
- Identification of the potential relationships for snow accumulation rate, trace element records in ice core with climate factors
- Retrieval of correlations between climate factors and indicators of large-scale atmospheric circulation (e.g., SAM, ASL) near Victoria Land
- Reconstruction of large-scale atmospheric circulation using ice core records

IV. R&D Results

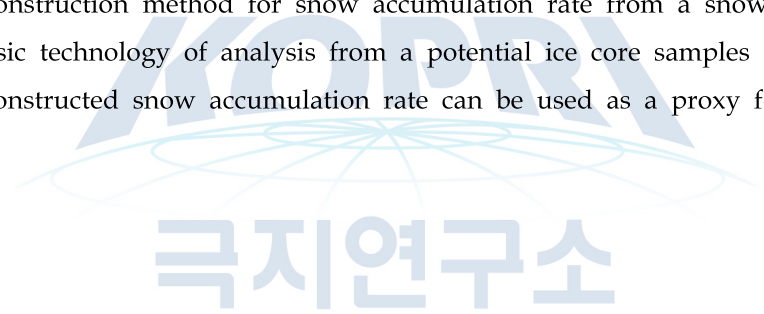
- Water stable isotopes and trace elements have been analyzed in the Styx firn core
- The age of the Styx firn cor (Styx-B) was estimated to be approximately 25-year based on the water isotopes, major ions, and firn densification modelling
- The age dating allow the estimation of snow accumulation rate which further

correlated the sea ice extent near the study area

- The variation of water isotopes and the decreasing snow accumulation in the Styx snowpit indicate the relation to the sea ice extent and lowering of air temperature in the study area
- The application of the ^{17}O isotopes to the ice core studies have been reviewed and examined
- The monthly mean water isotopic values in the Styx snowpit show similar trend with air temperature
- Trace elements have been analyzed in the portion of Styx ice core to compare with relevant climate factors
- Ice melting experiments have been performed to improve the interpretation of melt layers in ice cores

V. Application Plans of R&D Results

- The reconstruction method for snow accumulation rate from a snowpit and ice core can be a basic technology of analysis from a potential ice core samples
- The reconstructed snow accumulation rate can be used as a proxy for climate change

The logo for KOPRI (Korea Polar Research Institute) features a stylized globe with latitude and longitude lines. The acronym 'KOPRI' is written in large, blue, semi-transparent letters across the globe. Below the globe, the Korean text '극지연구소' (KOPRI) is written in a bold, blue font.

극지연구소

목 차

제 1 장 서론

제 2 장 국내외 기술개발 현황

제 3 장 연구개발수행 내용 및 결과

제 4장 연구개발목표 달성도 및 대외기여도

제 5 장 연구개발결과의 활용계획

제 6 장 연구개발과정에서 수집한 해외과학기술정보

제 7 장 참고문헌



본 문

(작 성 요 령)

1. 본문의 순서는 장, 절, 1, 가, (1), (가), ①, ②, 등으로 하고,
 - 장은 17 포인트 중고딕체
 - 절은 15 포인트 명조체
 - 본문은 11 포인트 신명조체로 한다.
단, 본문의 내용중 중요부문은 중고딕체로 사용할 수 있다.
2. 장은 원칙적으로 페이지를 바꾸어 시작한다.
3. 본문은 명조체 11 포인트 횡으로 작성한다.
4. 페이지 번호는 하단 중앙 끝에 11 포인트로 한다.
5. 각주는 해당 페이지 하단에 8포인트 활자로 표기하며, 본문과 구분토록 한다.
6. 페이지수는 편집순서 2의 제출문부터 시작한다.
단, 삽입물이 있을 때는 그 삽입물의 크기에 불문하고 1면을 한 페이지로 하여 일련번호를 붙인다.
7. 한글, 한문, 영문을 혼용할 수 있다.
8. 뒷면지에 주의문을 넣는다.
- 9.참고문헌(reference) 인용의 경우 본문 중에 사용처를 반드시 표시한다.

제 1장 서론

본 과제의 최종목표 및 3년간의 단계별 목표를 정리하면 다음과 같다. 국내외 관련분야와 최종목표와의 관련된 내용은 다음 장에 제시하였다.

□ 최종목표

| |
|--|
| <p>빙하시료를 이용한 남극 빅토리아 주변 강설량 복원 및 과거 기후인자와의 상관성을 통한 과거대기대순환 복원</p> <ul style="list-style-type: none"> - 천부빙하코어의 불안정동위원소를 이용한 연대측정 - 연대측정을 통한 빅토리아랜드 강설량 복원 - 강설량, 미량원소와 기후인자간의 상관성 파악 - 이러한 기후인자와 빅토리아랜드 주변의 대기대순환(SAM, ASL)등과의 상관성 확보 - 빙하코어시료를 이용하여 과거 대기대순환 복원 |
|--|

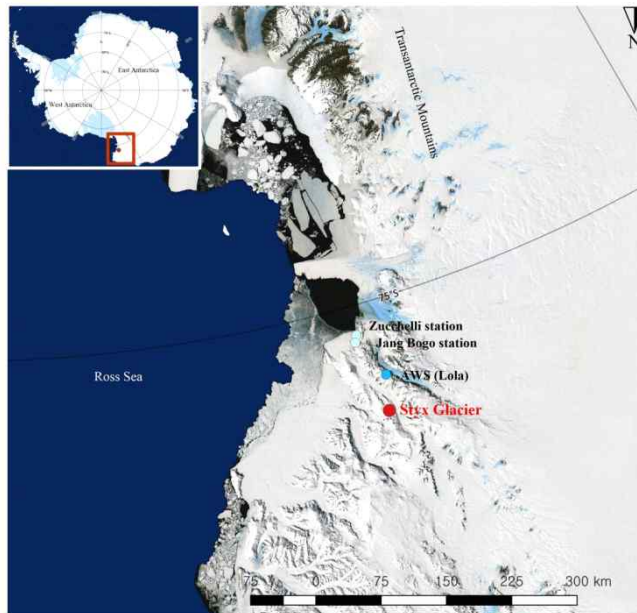
□ 연차별 연구목표

| 연차 | 연구 목표 | 연구 내용 | 비고 |
|------------|------------------------------------|-------------------------------------|----|
| 1차년도(2020) | 빙하코어시료의 불안정동위원소 분석 및 기후인자와의 상관성 분석 | 빙하코어시료의 안정동위원소분석 및 미량원소분석 | |
| | | 분석된 불안정동위원소를 이용하여 빙하의 연대측정 | |
| | | 빙하의 연대측정을 통한 강설량 복원 | |
| 2차년도(2021) | 기후인자와 대기대순환과의 상관성분석 | 복원된 강설량과 기후인자와의 상관성 파악 | |
| | | 기후인자와 대기대순환과의 상관성 연구 | |
| 3차년도(2022) | 빙하코어시료를 이용한 과거 대기대순환 복원 | 빙하코어시료와 대기대순환과의 상관성을 설명할 수 있는 프록시개발 | |
| | | 빙하코어시료로부터 과거대기대순환 복원 | |

제 2 장 국내외 기술개발 현황

2.1. 빅토리아랜드 주변 빙하코어시료

극지연구소에서는 남극 장보고기지 주변 북빅토리아랜드에 4개의 빙하코어시료를 확보하고 있다(그림). 남극 북빅토리아랜드 GV7 (2013-14 시즌, 80 m), Styx (2014-15 시즌, 210 m), Hercules Neve (2015-16 시즌, 80 m), Tourmaline plateau (2018-19 시즌, 65 m)에서 천부빙하코어를 성공적으로 시추하였다. 현재 GV7은 불안정동위원소를 이용하여 빙하의 연대측정만이 완료되어 있으며, Styx는 현재 빙하의 연대측정이 시도되고 있음. 나머지 두 연구지역은 아직 연대측정이 시도되고 있지 않았다. 이 지역은 주로 주변 로스해에서 기원한 수증기가 빅토리아랜드쪽으로 이동하는 것으로 알려져 있다. Stenni et al. (2000)에서는 이 지역에 눈이 잘 보존되어 있고 적설량이 상대적으로 다른 지역보다 높아 빙하연구에 적절한 지역으로 선정하였다. 상대적으로 적설량이 적은 내륙지역에서는 빙하의 안정동위원소가 주로 온도에 의해 결정되기 때문에 기온변화에 따른 연구만이 수행되어 왔지만, 빅토리아랜드 지역의 경우 강설량이 많고 주로 로스해에서 기원한 수증기이기 때문에 해양과 관련된 연구를 하기에는 좋은 연구지역으로 평가 받고 있다. 예를 들어, 해빙의 면적에 따라 불안정동위원소는 변동을 하기 때문에 빙하코어시료의 안정동위원소는 온도 뿐만 아니라 해빙의 면적에 의해서도 영향을 받는다. 따라서, 수학적 또는 화학적으로 적절한 자료처리를 통해 과거 해빙의 면적을 복원 해 볼 수도 있다.



<그림> 장보고기지 주변 Styx 빙하시료 위치

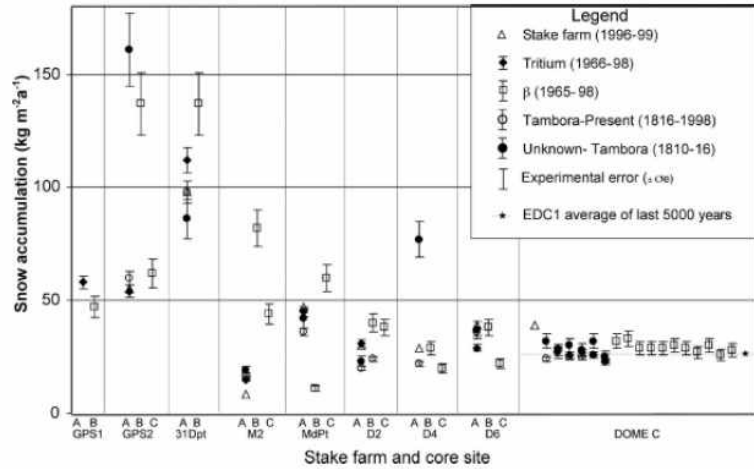
2.2. 강설량 복원

빙하코어시료를 분석하여 빙하코어의 연대를 안정동위원소분석을 통해 추정할 수 있다. 불안정동위원소의 계절성을 이용하면 안정동위원소 값은 싸인 함수를 가지게 되고 최대값과 최대값의 간격이 1년이 되게 된다. 이를 이용하여 최근 빙하코어 시료의 연대를 측정하게 되고 특정 사건을 이용하여 빙하코어시료의 연대를 확정할 수 있게 된다. 빙하코어시료의 연대가 확정되면 구간별 밀도를 이용하여 강설량을 물의 길이로 나타낼 수 있다. 특히 강설량 변동의 경우 남극 물순환에서 중요한 의미를 가질 수 있다. 특히, 해수면변동과도 밀접한 상관성이 있으며, 해안 주변에서 강설량의 변동은 남극에서의 얼음의 질량 문제(Antarctic mass balance)에도 많은 의미를 가질 수 있다.

극지역에서 강설량은 다양한 요인에 의해서 결정될 수 있다. 눈이 쌓인 뒤에 승화 또는 바람에 의해서 영향을 받을 수 있으며, 대기대순환의 변화에 의해서도 크게 영향을 받을 수 있다. 다음 표와 그림은 지역별로 강설량의 변동을 나타낸 것이다.

<표> 빅토리아랜드 주변의 평균적인 강설량

| Locations | Accumulation kg $m^{-2} y^{-1}$ | Time period | Reference |
|---|------------------------------------|-------------|--------------------------------|
| Styx-A core | 164±71 | 1951-2014 | Nyamgerel et al (submitted) |
| Styx-A core | 124±40 | 1990-2014 | |
| Styx-B core | 146±59 | 1990-2014 | |
| Hercules Neve, northern Victoria Land | 160 | 1971-1992 | Udisti, 1996 |
| Styx Glacier | 203 (111-335) | 1994-1970 | Stenni and others, 2000 |
| Talos Dome | 86.6 | 1965-2007 | Stenni and others, 2002 |
| Northern Victoria Land (GPS2) | 93±44 | - | Frezzotti and others, 2004 |
| Nearest to northern Victoria Land from traverse data (GV5/TDN) | 141/83.9 | 1998-2001 | Becagli and others, 2004 |
| Styx Glacier | 260 | 2009-2012 | Kwak and others, 2015 |
| Styx Glacier (model result in same core) | 130 | ~1360-2014 | Han and others, 2015 |
| GV7, northern Victoria Land | 242±71 | 2008-2013 | Caiazza and others, 2017 |



<그림> 트래버스를 하면서 측정한 강설량변화

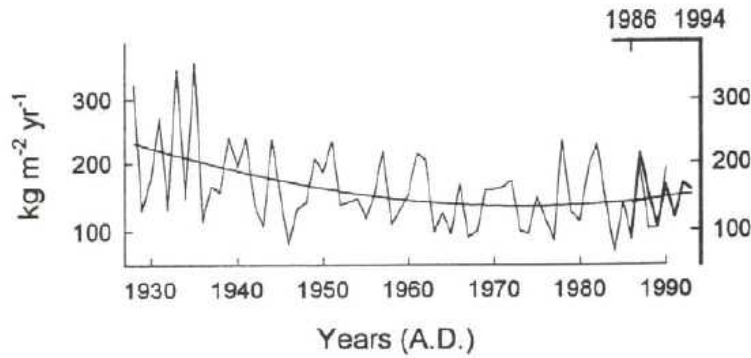


Fig. 4. Record of annual accumulation rate from the firn core (thin line, left and lower axes) and the snow pit (thick line, right and upper axes). The second-order correlation line shows the general variability in the accumulation trend.

<그림> 편코어에서의 강설량의 변동. 강설량 변동에 경향성이 있음

국내에서도 Styx 지역의 편코어를 이용해서 연대측정을 시도하였고 이후 강설량을 추정하여 모델결과와 비교를 시도하였다(그림). Thomas et al. (2017)에서는 남극 빙상의 질량이 증가하였는데, 이를 해안 주변에서의 최근 강설량의 증가를 원인으로 지목하였다. 최근 10년간 평균보다 $123 \pm 44 \text{ Gt yr}^{-1}$ 만큼 증가하여 표면 질량의 변화 원인을 추정하면서, 고도가 낮은 해안지역을 주목하였다(그림). 이는 지역별 강설량 자료와 재분석자료(Reanalysis)와 모델결과를 이용한 결과를 비교하였다.

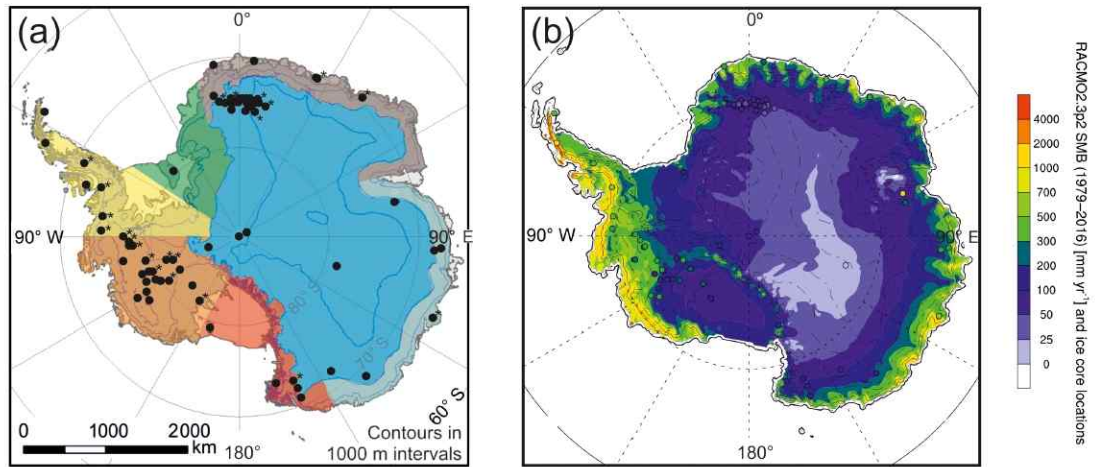
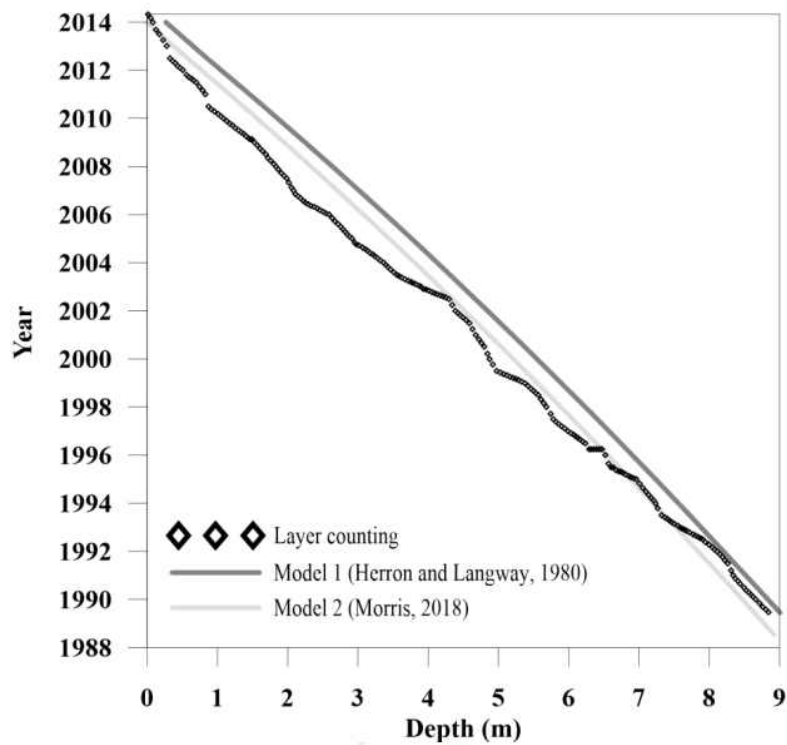


Figure 1. (a) Location of all ice cores and the regional boundaries used in this study. EAP (blue), WL (cyan), WS (green), AP (yellow), WAIS (orange), VL (red), and DML (brown). Stars denote sites where correlation between ice core snow accumulation and RACMO2.3p2 SMB is significant at $p < 0.05$. (b) RACMO2.3p2 SMB (1979–2016) overlain with ice core SMB since 1979 at each location.

<그림> 해안가의 강설량 중요성을 나타내는 연구결과



<그림> 모델과의 비교를 통한 강설량 추정

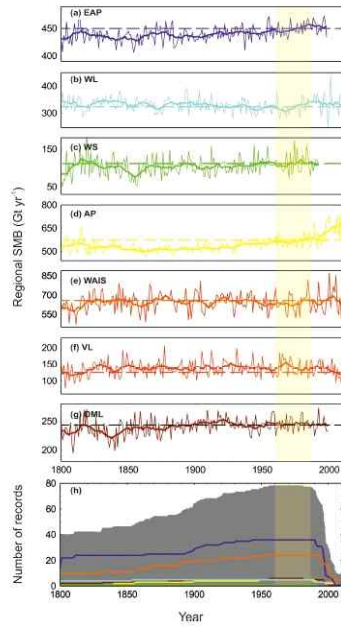


Figure 6. Regional SMB composites (1800–2010 AD) shown as annual averages (thin lines) and 5-year means (thick lines) for (a–g) the East Antarctic Plateau (EAP, dark blue); Wilkes Land coast (WL, cyan), Weddell Sea coast (WS, green), Antarctic Peninsula (AP, yellow), West Antarctic Ice Sheet (WAIS, orange), Victoria Land (VL, red), and Dronning Maud Land (DML, brown). Panel (h) represents the total number of records (solid grey) and the number of records by region.

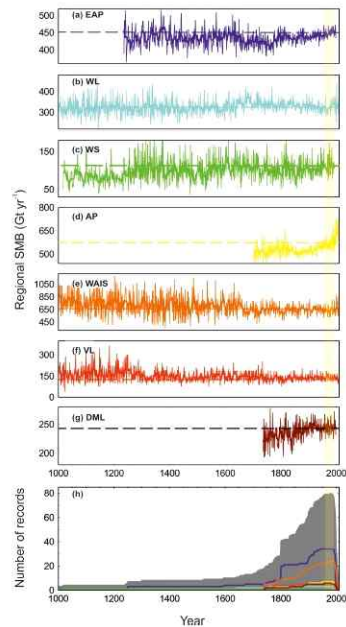


Figure 7. Regional SMB composites (1000–2010 AD) shown as annual averages (thin lines) and 10-year running means (thick lines) for (a–g) the East Antarctic Plateau (EAP, dark blue); Wilkes Land coast (WL, cyan), Weddell Sea coast (WS, green), Antarctic Peninsula (AP, yellow), West Antarctic Ice Sheet (WAIS, orange), Victoria Land (VL, red), and Dronning Maud Land (DML, brown). Panel (h) represents the total number of records (solid grey) and the number of records by region.

<그림> 최근 200년(좌)과 1000년(우)의 극지적인 남극 강설량 비교

2.3. Amundsen Sea Low (ASL)과 남극진동(Southern Annular Mode, SAM)

ASL은 남극과 로스해 주변에서 발생하는 저기압 시스템이다. ASL에 의해 서남극은 표면에서의 온도, 바람속도, 강수량 및 해빙의 면적이 영향을 받는 것으로 알려져 있다. 다음 그림에서는 로스해 주변에서 ASL가 어떻게 강설량에 영향을 주는 지에 대하여 제시되어 있다. 1990–2014 동안 로스해에서는 해빙의 면적이 증가가 여러 빙하연구에서 제시되었다. 이는 양의 남극진동과 ASL의 장소로 인해 빅토리아랜드의 기온이 감소하였다. Styx의 강설량 자료에서는도 지난 20년 동안 강설량감소가 잘 나타나고 있다(그림). 이러한 기후변동은 해빙의 면적과 밀접히 관련이 있으며, 다음과 같은 기작으로 설명할 수 있다. 해빙의 면적이 감소하면 증발이 많이 되어 주변 지역의 강설량이 증가하게 된다. 따라서, 수분의 발생 경로 및 이동거리가 달라지게 되면 눈의 안정동위원소 값에 변화가 발생하여 빙하코어시료를 이용하여 과거의 고기후를 복원하게 될 때 고려해야 할 요인이 온도 이외에 추가되게 된다. 또한, 빙하코어시료에 화학성분(미량원소 및 주요이온) 중에서 해양에서 유도되는 것은 해빙의 면적을 복원하는데에 도움을 줄 수 있다(그림)

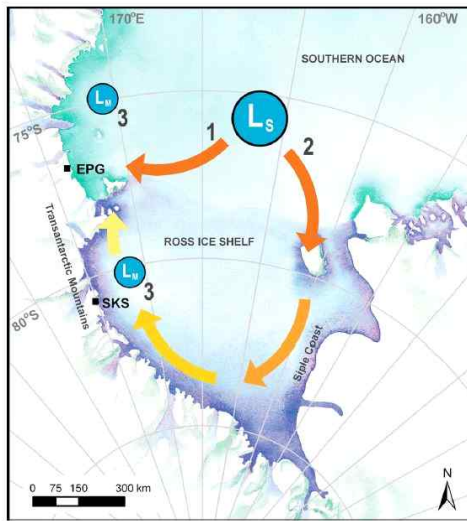


Figure 7. A schematic diagram of three mechanisms of snow delivery to the western margin of the Ross Sea and ice core sites, SKS and EPG: (1) low-pressure systems (L_S) that track around the margin of the continent bringing moist marine air; (2) low-pressure systems that sweep across the Ross Ice Shelf and are constrained by the inland topography, bringing high accumulation to inland sites and less snow at more northern sites; and (3) mesocyclones (L_M) bringing short-duration pulses of snow particularly near the Byrd Glacier and in the Terra Nova Bay region.

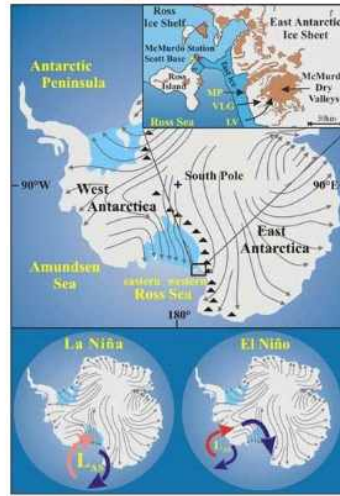
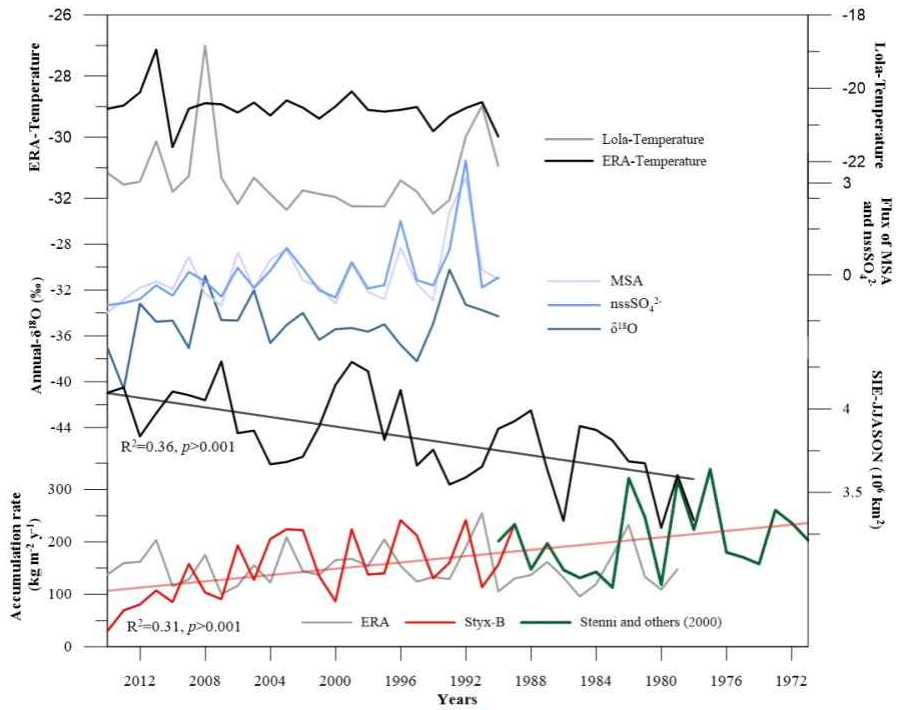
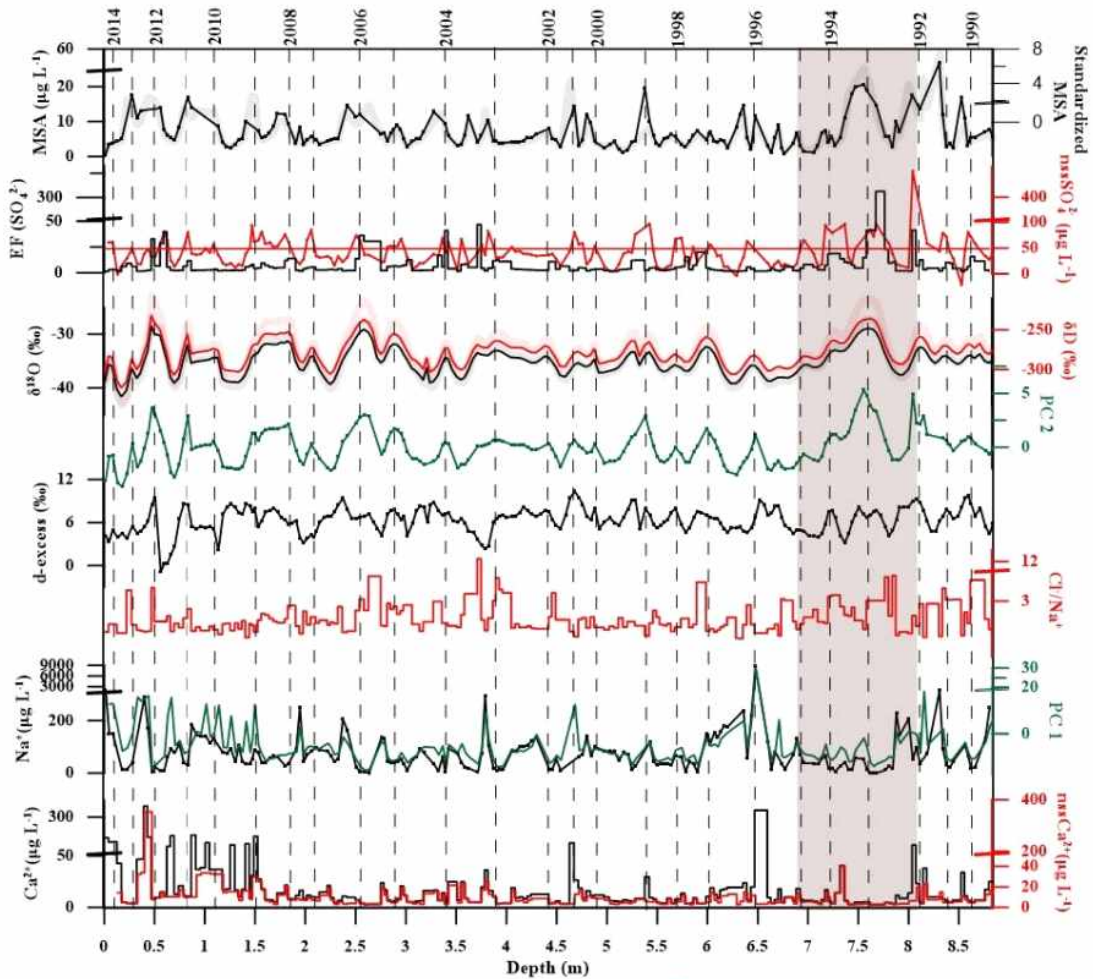


Figure 1. Map of surface wind pattern in Antarctica (modified after King and Turner, 1997). Grey arrows indicate wind flow direction. Triangles represent Transantarctic Mountain range. Top inset: McMurdo Sound region and location of the McMurdo Dry Valleys; Marble Point (MP), Victoria Lower Glacier (VLG), and Lake Vida (LV). Bottom inset: typical position of Amundsen Sea Low (L_{AS}) during La Niña and El Niño events (modified after Cullather et al., 1996). Red arrows indicate relatively warm airmasses (even warmer during El Niño) and blue arrow indicates cold airmasses. The size of ' L_{AS} ' indicates its strength.

<그림> 로스해 주변 강설량 기작 및 표면에서의 바람장에 대한 지도



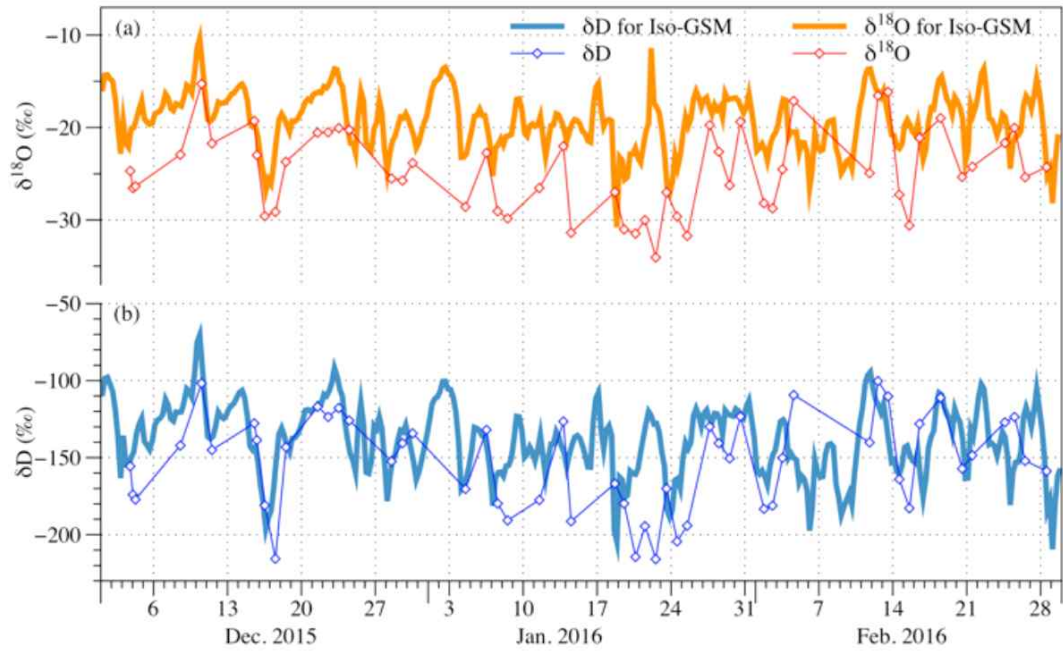
<그림> Styx 강설량 및 동위원소 결과



<그림> Styx 지역 편코어의 화학성분 변화

2.4. 본 연구과제와의 상관성

극지연구소의 본 과제는 “국제심부빙하시추 네트워크를 활용한 대기-빙상 상호작용의 자연적, 인위적 특성규명”이며, 국제네트워크의 일원으로 빙하코어시추에 참가하여 쌓은 경험으로 남극 내륙기지 및 심부빙하시추 기술을 습득하는 것을 목표로 하고 있다. 또한, 천부빙하코어를 이용하여 빅토리아랜드 주변의 자연적, 인위적인 변동을 고해상도로 복원하는 것이 목표이다. 본 연구에서는 심부빙하시추에 참가하여 얻은 천부빙하코어를 이용하여 심부빙하코어를 해석하는데 도움을 줄 수 있을 것으로 판단된다. 빅토리아랜드에서 확보한 빙하코어시료는 자연적인 기상변동과 강설량의 상관성을 찾을 수 있으면, 과거 기후변화의 프록시로 강설량을 활용할 수 있을 것으로 판단된다. 위에서 언급한 것처럼, 주변 대기대순환에 의해 해빙의 면적이 결정되면, 이는 눈 동위원소에 변화를 발생시켜 온도 이외에도 동위원소 변동을 설명할 수 있는 요인이 될 것이다. 동위원소를 포함한 화학성분을 주성분 분석(principal component analysis)을 통하여 화학성분에 가장 영향을 주는 요인을 선별할 수 있을 것으로 기대된다. Iso-GSM모델(동위원소가 포함되어 있는 대기대순환모델) 결과와 빙하코어시료에서 얻은 눈 동위원소 값을 비교하여 향후 동위원소모델의 활용 가능성을 타진 해 볼 것이다.



<그림> Iso-GSM과 직접 포획한 수증기동위원소와의 비교 연구



제 3 장 연구개발수행 내용 및 결과

앞 장에서 제시한 연구목표를 달성하기 위하여 다음과 같이 연구를 수행하였다.

| 성과목표 | 세부목표 | 연구수행방법 (이론적·실험적 접근방법) | 구체적인 내용 |
|---|---|--|----------|
| 빙하코어시료의 안정동위원소 분석 및 기후인자와의 상관성 분석 | 빙하코어시료의 안정동위원소분석 및 미량원소분석 | - 스틱스지역의 편(firm) 코어의 물안정동위원소분석을 완료하였 으며, 현재 미량원소분석을 수행 하고 있음 | |
| | 분석된 안정동위원소를 이용하여 빙하의 연대측정 | - 스틱스빙하시료의 안정동위원 소 및 주요이온, 모델결과를 활 용하여 25년의 연대를 추정하였 음 | |
| | 빙하의 연대측정을 통한 강설량 복원 | - 빙하의 연대측정을 통한 스틱 스지역의 강설량을 추정하여 해빙과의 상관관계를 밝혔음 | |
| 기후인자와 대기대순환과 의 상관성분석 | 복원된 강설량과 기후인자와의 상관성 파악 | - 스노우팻 시료를 이용하여 해 빙의 면적과 안정동위원소 값 에 상관성이 있음을 밝혔음 - ¹⁷ O의 빙하연구 가능성에 대하 여 타진하였음 | 아래 내용 참조 |
| | 기후인자와 대기대순환과의 상관성 연구 | - 스노우팻을 이용하여 월평균안 정동위원소 값이 대기온도와 상관관계가 있음을 밝혔음 | |
| 빙하코어시료 를 이용한 과거 대기대순환 복원 | 빙하코어시료와 대기대순환과의 상관성을 설명할 수 있는 프록시개발 | - 빙하코어의 미량원소분석 결과 를 향후 기상자료와 비교하기 위 하여 스틱스지역에서 가져온 편 코어의 미량원소 분석결과 분석 및 정리. - 빙하코어의 melting layer 해 석하기 위해 얼음 용해 실험 수 행하였음. | |
| | 빙하코어시료로부 터 과거대기대순환 복원 | - 자료 분석 및 정리 | |

3.1. 남극 북빅토리아 스틱스 빙하의 연대추정을 통한 강설량 계산

빙하시료의 연대추정은 과거의 환경, 기후 및 대기순환의 기록을 복원하는 데 가장 기본적인 과정이다(Legrand and Mayewski, 1997; Traversi and others, 2004; Sinclair and others, 2010; Furukawa and others, 2017). 따라서, 본 연구에서도 과거의 기후 및 대기조건을 복원하기 위하여, 남극에서 해안에서 상대적으로 가까운 스틱스빙하(73° 50.975' S, 163° 41.640' E; 1623 m a.s.l.)를 이용하였다. 8.84미터의 편코어를 이용하여 연대추정으로부터 강설량을 추정하였다.

통계적인 요약은 아래 표에 제시하였으며, 편코어를 분석한 화학자료에 주성부분석을 적용하였으며, 이 역시 아래 표에 제시하였다. 편코어분석자료의 시간적 변동은 아래 그림에 제시하였다. 편코어의 화학적, 동위원소적인 자료를 이용하여 추정한 연대와 편코어가 축적되는 과정을 이용한 모델계산을 비교하여 그림으로 나타내었다. 또한, 기온, 해빙의 면적, 강설량의 시간적인 변동도 아래 그림에 나타내었다.

1990년부터 2014년까지 물동위원소와 화학성분을 이용하여 편코어의 연대를 추정하였으며, 화산신호인 황산염으로 검증하였다. 강설량은 대체적으로 감소하는 경향을 보였으며, 평균은 $146 \pm 60 \text{ kg m}^{-2} \text{ y}^{-1}$ 로 추정되었다. 이는 로스해 주변의 빙붕면적과 관련이 있어 보이며, 이는 향후 보다 긴 빙하코어 시료를 해석하는 데에 도움이 될 것으로 판단된다.

Table 3.1.1. Summary of statistics of water stable isotopes in ‰ ($n = 227$) and chemical species in $\mu\text{g L}^{-1}$ ($n = 197$) in the firm core.

| | Min | Max | Range | Mean | Media | Std. | Std. | Mean nss |
|-----------------------|--------------------|----------|----------|--------------------|--------------------|-------|-----------|----------|
| | | | | | n | error | deviation | % |
| $\delta^{18}\text{O}$ | - 43.13 - 340.6 | - 26.70 | 16.43 | - 34.92 - 273.1 | - 34.85 - 272.9 | 0.21 | 3.13 | - - |
| δD | 3 | - 205.17 | 135.46 | 1 | 9 | 1.68 | 25.32 | - |
| MSA | 1.34 | 53.71 | 52.37 | 8.12 | 5.25 | 0.51 | 7.17 | - |
| Cl^{-} | 6.58 | 16394.61 | 16388.03 | 339.42 | 151.98 | 88.34 | 1239.98 | 25.1 |
| SO_4^{2-} | | | | | | | | 65.5 |
| - | 13.38 | 2506.58 | 2493.20 | 91.63 | 65.80 | 13.43 | 188.53 | |
| Na^{+} | 1.20 | 8802.32 | 8801.12 | 171.07 | 64.45 | 47.81 | 671.04 | (a)- |
| K^{+} | 0.43 | 373.13 | 372.70 | 7.38 | 2.61 | 2.04 | 28.60 | 19.2 |
| Mg^{2+} | 1.07 | 1042.42 | 1041.35 | 20.86 | 10.01 | 5.53 | 77.67 | 19.1 |
| Ca^{2+} | 2.73 | 362.57 | 359.83 | 26.97 | 9.91 | 3.64 | 51.08 | 74.0 |

(a) assumed to be solely sourced from sea spray

Table 3.1.2. Loadings of 11 variables for first three principal components (PC) in the firm core with larger values highlighted in bold.

| | PC 1 | PC 2 | PC 3 |
|-----------------------|--------|-------------|-------------|
| $\delta^{18}\text{O}$ | - 0.12 | 0.92 | - 0.24 |
| δD | - 0.12 | 0.93 | - 0.17 |
| d-excess | - 0.03 | 0.33 | 0.92 |
| MSA | 0.15 | 0.60 | 0.09 |

| | | | |
|----------------------------------|-------|-------------|--------|
| Cl ⁻ | 0.99 | - 0.01 | 0.02 |
| ssSO ₄ ²⁻ | 0.99 | - 0.01 | 0.02 |
| nssSO ₄ ²⁻ | 0.33 | 0.60 | 0.01 |
| Na ⁺ | 0.99 | - 0.01 | 0.02 |
| K ⁺ | 0.99 | - 0.02 | - 0.01 |
| Mg ²⁺ | 0.99 | 0.00 | 0.02 |
| Ca ²⁺ | 0.62 | - 0.03 | - 0.19 |
| Variance explained (%) | 49.52 | 23.14 | 8.86 |
| Cumulative percent (%) | 49.52 | 72.66 | 81.52 |
| Number of variables | 197 | 197 | 197 |

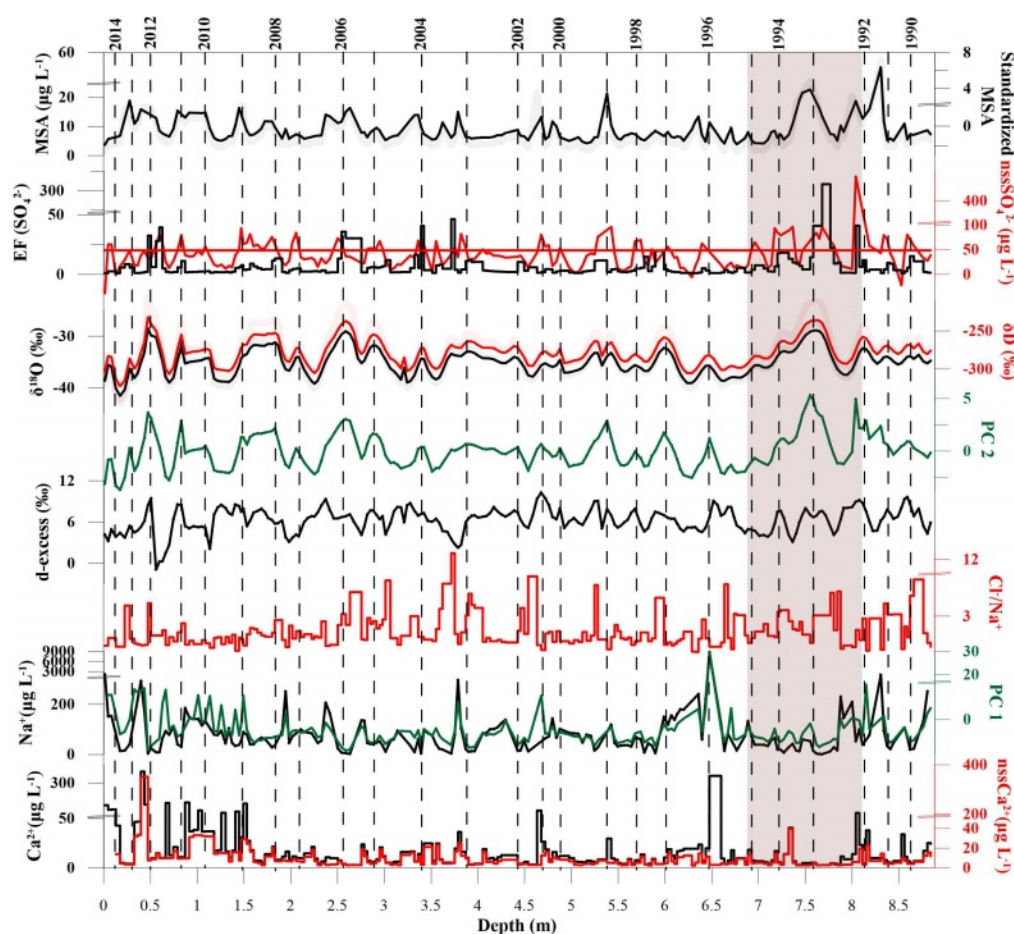


Fig 3.1.1. Annual layer counting of the isotopic and ionic species with PC 1 and PC 2 score, starting from the year of drilling (2014). The Cl⁻, Mg²⁺, K⁺ are not shown in the figure because those are similar to Na⁺ ($r > 0.99$), but the ratio of Cl⁻/Na⁺ shown. Non-sea-salt portions are indicated for Ca²⁺. The raw values (wide line) of $\delta^{18}\text{O}$, δD , and MSA shown with standardized profile in thin line. Enrichment factor (EF) of nssSO₄²⁻ was shown in black line and horizontal red line indicate the average nssSO₄²⁻. Brown shading represent depth range to increased nssSO₄²⁻ which indicate the period of Pinatubo and Cerro Hudson volcanic signals.

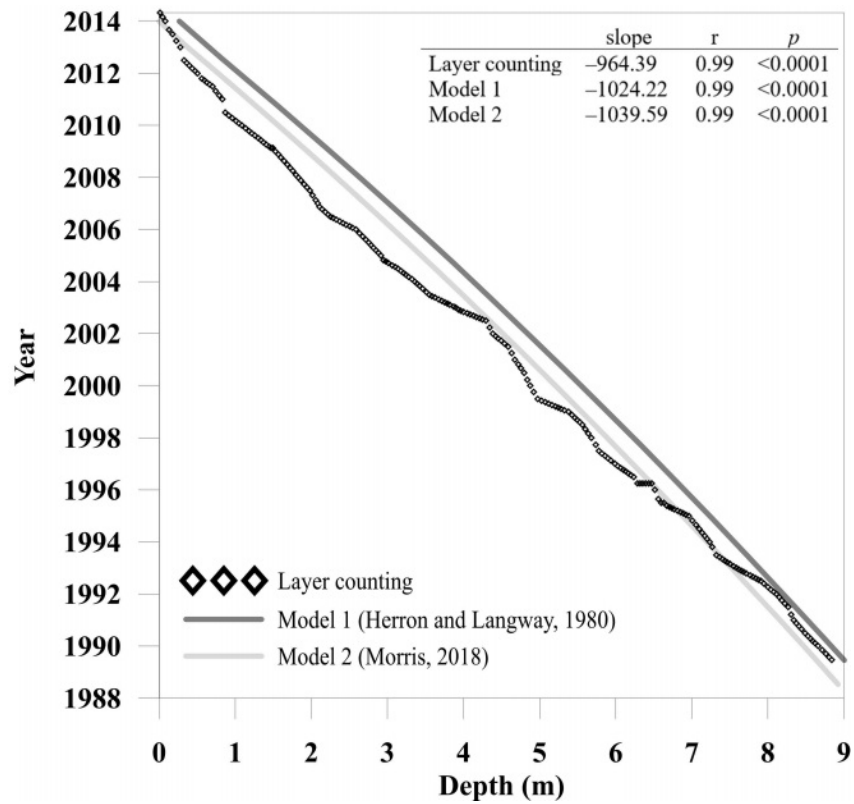


Fig 3.1.2. The comparison of the depth-age relationship of the annual layer counting and the firn densification models.

Table 3.1.3. Mean accumulation rates estimated near to the Styx glacier for comparison to the firn core

| Locations | Accumulation rate, $\text{kg m}^{-2} \text{y}^{-1}$ | Time period | Reference |
|--|---|--------------|--------------------------|
| Styx Glacier | 146 ± 60 | 1990 - 2014 | This study |
| ERA-Interim | 154 ± 37 | 1990 - 2014 | Dee and others, 2011 |
| ERA-Interim | 150 ± 36 | 1979 - 2014 | |
| Hercules Neve | 160 | 1971 - 1992 | Udisti, 1996 |
| Styx Glacier | 203 (111-335) | 1971-1990 | Stenni and others, 2000 |
| Talos Dome | 86.6 | 1965 - 2007 | Stenni and others, 2002 |
| Styx Glacier | 226 | 2009 - 2012 | Kwak and others, 2015 |
| Styx-M (densification model for Styx-M-core) | 130 | ~1360 - 2014 | Han and others, 2015 |
| GV7 | 242 ± 71 | 2008 - 2013 | Caiazza and others, 2017 |

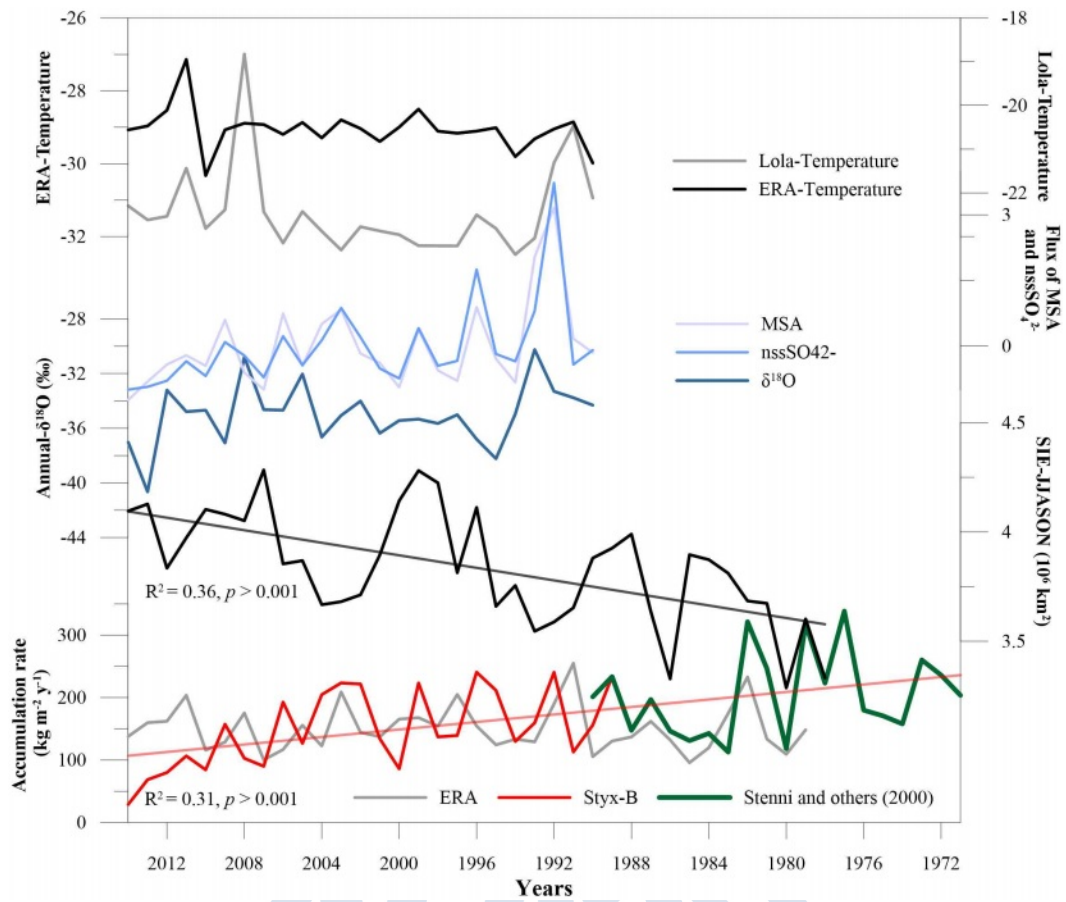


Fig 3.1.3. Comparison of annual accumulation rate (Styx-B firn core, ERA-interim, Stenni and others, 2000), annual mean $\delta^{18}\text{O}$, standardized annual flux of MSA and nssSO_4^{2-} , SIE during cold period (JJASON) and temperature record from Lola AWS and ERA-Interim reanalysis data. The linear trendlines shown for annual accumulation rate (Styx-B firn core for the period of 1990–2014 together with Stenni and others (2000) up to 1971 from 1990) and trend of SIE between 1979 and 2014)

위의 내용은 다음의 논문으로 출판되었다.



Chronological characteristics for snow accumulation on Styx Glacier in northern Victoria Land, Antarctica

Article

Cite this article: Nyamgerel Y, Han Y, Kim S, Hong S-B, Lee J, Hur SD (2020). Chronological characteristics for snow accumulation on Styx Glacier in northern Victoria Land, Antarctica. *Journal of Glaciology* 66(260), 916–926. <https://doi.org/10.1017/jog.2020.53>

Received: 30 November 2019
Revised: 25 June 2020
Accepted: 26 June 2020
First published online: 26 August 2020

Key words:

Annual layer counting; ionic species; snow accumulation; stable water isotopes; Styx Glacier

Author for correspondence:

Jeonghoon Lee,
E-mail: jeonghoon.d.lee@gmail.com

Yalalt Nyamgerel^{1,2}, Yeongcheol Han², Songyi Kim^{1,2}, Sang-Bum Hong², Jeonghoon Lee¹ and Soon Do Hur²

¹Department of Science Education, Ewha Womans University, Seoul 120-750, Korea and ²Division of Paleoenvironment, Korea Polar Research Institute, Incheon, 21990, Korea

Abstract

Under the potential to reconstruct the past climatic and atmospheric conditions from a deep ice core in the coastal Antarctic site (Styx Glacier), an 8.84 m long firn core (73°50.975' S, 163°41.640' E; 1623 m a.s.l.) was initially studied to propose a reliable age scale for the local estimation of snow accumulation rate. The seasonal variations of $\delta^{18}\text{O}$, methanesulfonic acid (MSA) and non-sea-salt sulfate (nssSO_4^{2-}) were used for the firn core dating and revealed 25 annual peaks (from 1990 to 2014) with volcanic sulfate signal. The observed declining trend in annual accumulation rate with a mean value of $146 \pm 60 \text{ kg m}^{-2} \text{ a}^{-1}$ is likely to be linked to the changes of sea-ice extent in the Ross Sea region. Moreover, the temporal variation of the annual mean $\delta^{18}\text{O}$, an annual flux of MSA and nssSO_4^{2-} also likely to be under the influence of ice-covered and open water area. This study suggests a potential to recover past changes in an oceanic environment and will be useful for the interpretation of the long ice core drilled at the same site.

3.2. 남극 해안가 주변의 스노우핏의 기상학적인 특성

스틱스지역에서 획득한 스노우핏 시료를 이용하여 4년간의 기상학적인 특성에 대한 연구를 수행하였다. 본 연구는 2021년 *Earth Interactions*에 출판되었다. 논문에서 중요한 부분을 발췌한 것을 아래에 제시하였다.

Polar snowpits or ice cores preserve valuable information derived from atmosphere on past climate and environment changes. Due to the significant spatial and temporal variabilities in Antarctic snowfall and temperature (Ingólfsson et al. 2003; Anschütz et al. 2007; Frezzotti et al. 2007; Masson-Delmotte et al. 2008; Yang et al. 2018) and the sparse collection of weather stations (Stenni et al. 2000; Tuohy et al. 2015), there are still limitations on the interpretation of paleoclimate records. Caiazzo et al. (2016) stated that the temporal variability is more directly correspond to the real environmental changes rather than spatial variability of the site. Thus, a site-based information and evaluation of isotopic and chemical compositions are required to investigate the present-day snow compositions and its differences at regional and/or local scales, and application to the interpretation of the paleoclimate records (Stenni et al. 2000; Ingólfsson et al. 2003; Tuohy et al. 2015; Stenni et al. 2017).

A 1.57 m snowpit recovered from the coastal site (Styx Glacier) in Eastern Antarctica during the 2014/2015 Antarctic expedition by the KOPRI and was discussed and compared with meteorological variables. The purpose of this study is to evaluate

the isotopic ($\delta^{18}\text{O}$ and δD) and ionic composition (Na^+ , K^+ , Mg^{2+} , Ca^{2+} , MSA , Cl^- , NO_3^- and SO_4^{2-}) of the snowpit by comparing with instrumental meteorological variables in the seasonal scale. It is beneficial to understand the seasonality in potential and dominant climate factors, which alter the snowpit record in this location. This work reports the most recent and high-resolution snowpit record in the Styx Glacier. Our results will support the previous records reported (Udisti et al. 1998; Stenni et al. 2000; Traversi et al. 2004; Kwak et al. 2015) and further interpretation of long cores from this site.

The range of isotopic and ionic values were shown and compared in table 2.1 and figure 2.1. The correlation matrix shown in table 2.2. Comparison of linear regression values of ions in the snowpit and reference seawater data shown in table 2.3. Figure 2.2. and table 2.4. represent the comparison of the snowpit records with climate variables. Dominant contribution of sea salt aerosols deposition due to the proximity of the site to the ocean and processes of sea ice formation was revealed in the ionic concentrations. Consistent seasonal peaks in $\delta^{18}\text{O}$, δD , MSA , nssSO_4^{2-} , and NO_3^- indicate the strong enhancement of their source during warm period, while the sea salt ions (Na^+ , K^+ , Mg^{2+} , Ca^{2+} , Cl^- and totSO_4^{2-}) exhibit a different distribution. Monthly mean $\delta^{18}\text{O}$ positively correlates with the air temperature record from AWS located in the main wind direction. Despite the shortness of the record, we suspect that the slight depletion of the isotopic composition and lowering of the snow accumulation could have related to the cooler air temperature with decreasing of open sea area. Consistency with previous studies and the positive correlation of sea salt ions in the snowpit indicate the relatively well preservation of snow layers with noticeable climate and environmental signals (e.g. changes in SIE or sea surface temperature). We report a new snowpit record which would be comparative and supportive to understand similar signals preserved in deeper ice cores in this location.

Table 3.2.1 Statistics of the isotopes and ions from different studies in northern Victoria Land

| | Stenni et al. 2000 | Gragnani et al. 1998 | This study | Nyamgerel et al. 2020 | Stenni et al. 2000 | Stenni et al. 2000 | Severi et al. 2009 |
|---|--------------------|----------------------|--------------|-----------------------|--------------------|--------------------|--------------------|
| Time period | 1980 - 1987 | 1986 - 1994 | 2010-2014 | 1990 - 2014 | 1971 - 1990 | 1973 - 1992 | |
| Type of record | Firn core | Firn core | Snowpit | Firn core | Firn core | Firn core | Ice core |
| Accumulation rate, $\text{kg m}^{-2} \text{y}^{-1}$ | 130 - 426 | 140 - 180 | 143.71 | 146 | 111 - 335 | 83 - 265 | 77.4 |
| Altitude, m a.s.l | 650 | 1560 | 1630 | 1630 | 1800 | 3000 | 2316 |
| Distance from coast, km | 40 | ~70 | ~60 | ~60 | 50 | 75 | 250 |
| Location | McCarthy Ridge | Campbell Glacier C | Styx Glacier | Styx Glacier | Styx Glacier | Hercules Neve | Talos Dome |
| $\delta^{18}\text{O}$ (‰) | Mean | | | | | | |
| | SD | | | | | | |
| | -25.5 | -33.5 | -36.16 | -34.92 | -32.9 | -33.6 | - |
| | 4.4 | | 5.02 | 3.13 | 3.2 | 2.4 | - |

| | | | | | | | | |
|--|------|-------|---------|----------|----------|-------|-------|-------|
| | Max | -17.1 | -27.2 | -24.90 | -26.70 | -23.7 | -27.0 | - |
| | Min | -37 | -40.8 | -43.91 | -43.13 | -39.2 | -42.0 | - |
| MSA (µg/l) | Mean | 26.7 | 16.17 | 14.12 | 8.12 | 13.6 | 94 | 5.36 |
| | SD | 24.4 | 12.36 | 15.78 | 7.17 | 10.1 | 6.9 | 6.61 |
| | Max | 143.0 | 71.32 | 66.08 | 53.71 | 57.3 | 118.3 | 40.49 |
| | Min | 2.0 | 3.80 | 2.03 | 1.34 | 2.5 | 12.7 | 0.42 |
| nssSO ₄ ²⁻ (µg/l) | Mean | 131.6 | 62.44 | 44.36 | 49.87 | 57.5 | 46.2 | 42 |
| | SD | 92.8 | 76.85 | 37.82 | 49.22 | 36.0 | 27.8 | 27.47 |
| | Max | 405.9 | 408.27 | 163.28 | 523.03 | 270.4 | 178.6 | 100.2 |
| | Min | 5.2 | -273.78 | 5.00 | 4.10 | 1.7 | 0.8 | 6.59 |
| Na ⁺ (µg/l) | Mean | - | 485.07 | 59.23 | 171.07 | - | - | 21.79 |
| | SD | - | 625.30 | 1480.14 | 671.04 | - | - | 16.14 |
| | Max | - | 4620.79 | 6706.94 | 8802.32 | - | - | 84.87 |
| | Min | - | 20.69 | 1.16 | 1.20 | - | - | 2.52 |
| Ca ²⁺ (µg/l) | Mean | - | 82.16 | 24.56 | 26.97 | - | - | 2.80 |
| | SD | - | 54.11 | 52.04 | 51.08 | - | - | 1.88 |
| | Max | - | 402.78 | 236.13 | 362.57 | - | - | 20.71 |
| | Min | - | 18.04 | 2.77 | 2.73 | - | - | 0.76 |
| K ⁺ (µg/l) | Mean | - | 144.66 | 20.47 | 7.38 | - | - | - |
| | SD | - | 191.58 | 57.15 | 28.60 | - | - | - |
| | Max | - | 1266.78 | 275.63 | 373.13 | - | - | - |
| | Min | - | 19.55 | 0.84 | 0.43 | - | - | - |
| Mg ²⁺ (µg/l) | Mean | - | 44.96 | 61.58 | 20.86 | - | - | 2.31 |
| | SD | - | 60.76 | 165.31 | 77.67 | - | - | 1.63 |
| | Max | - | 466.66 | 768.47 | 1042.42 | - | - | 10.56 |
| | Min | - | 8.51 | 1.49 | 1.07 | - | - | 0.36 |
| Cl ⁻ (µg/l) | Mean | - | 808.33 | 1018.27 | 339.42 | - | - | 46.73 |
| | SD | - | 1052.95 | 2672.45 | 1239.98 | - | - | 30.72 |
| | Max | - | 6877.88 | 12205.73 | 16394.61 | - | - | 184.1 |
| | Min | - | 88.63 | 7.30 | 6.58 | - | - | 6.54 |
| SO ₄ ²⁻ (µg/l) | Mean | - | 182.52 | 178.20 | 91.63 | - | - | 47.52 |
| | SD | - | 158.50 | 373.67 | 188.53 | - | - | 27.47 |
| | Max | - | 979.84 | 1732.80 | 2506.58 | - | - | 139.6 |
| | Min | - | 43.23 | 14.08 | 13.38 | - | - | 12.42 |
| NO ₃ ⁻ (µg/l) | Mean | - | 60.14 | 49.28 | 42.46 | - | - | 47.38 |
| | SD | - | 26.04 | 24.42 | 19.15 | - | - | 13.49 |
| | Max | - | 189.73 | 130.7 | 118.91 | - | - | 100.2 |
| | Min | - | 12.40 | 12.68 | 10.09 | - | - | 21.59 |

Table 3.2.2. Correlation matrix for the isotopic and ionic species in the snowpit. The correlation coefficient values larger than 0.4 were highlighted in bold ($n = 32$)

| | $\delta^{18}\text{O}$ | δD | d-excess | MSA | Cl^- | nss SO_4^{2-} | SO_4^{2-} | NO_3^- | Na^+ | K^+ | Mg^{2+} | Ca^{2+} |
|------------------------|-----------------------|------------------|--------------|-------------|---------------|------------------------|--------------------|-----------------|---------------|--------------|------------------|------------------|
| $\delta^{18}\text{O}$ | 1.00 | | | | | | | | | | | |
| δD | 1.00 | 1.00 | | | | | | | | | | |
| d-excess | -0.19 | -0.11 | 1.00 | | | | | | | | | |
| MSA | 0.41 | 0.45 | 0.35 | 1.00 | | | | | | | | |
| Cl^- | 0.11 | 0.12 | 0.02 | -0.15 | 1.00 | | | | | | | |
| nss SO_4^{2-} | 0.56 | 0.57 | 0.02 | 0.63 | 0.05 | 1.00 | | | | | | |
| tot SO_4^{2-} | 0.17 | 0.18 | 0.02 | -0.08 | 0.99 | 0.15 | 1.00 | | | | | |
| NO_3^- | 0.31 | 0.28 | -0.43 | -0.02 | 0.03 | 0.42 | 0.07 | 1.00 | | | | |
| Na^+ | 0.12 | 0.12 | 0.02 | -0.14 | 1.00 | 0.04 | 0.99 | 0.03 | 1.00 | | | |
| K^+ | 0.35 | 0.12 | 0.02 | -0.14 | 1.00 | 0.05 | 1.00 | 0.03 | 1.00 | 1.00 | | |
| Mg^{2+} | 0.11 | 0.12 | 0.03 | -0.14 | 1.00 | 0.06 | 1.00 | 0.02 | 1.00 | 1.00 | 1.00 | |
| Ca^{2+} | 0.14 | 0.15 | 0.00 | -0.14 | 0.99 | 0.11 | 0.99 | 0.07 | 0.99 | 0.99 | 0.99 | 1.00 |

Table 3.2.3. Linear regression of Na^+ versus K^+ , Mg^{2+} , Ca^{2+} and Cl^- with comparison to their theoretical ratios in seawater (Pilson, 2013)

| | Cl^- | ss SO_4^{2-} | Mg^{2+} | K^+ | Ca^{2+} |
|-----------------|---------------|-----------------------|------------------|--------------|------------------|
| Sea water ratio | 1.794 | 0.252 | 0.119 | 0.037 | 0.038 |
| Slope | 1.805 | 0.251 | 0.112 | 0.038 | 0.035 |
| Intercept | 44.734 | 42.87 | 1.444 | -0.346 | 5.75 |
| R^2 | 0.999 | 0.989 | 0.997 | 0.999 | 0.983 |
| n | 32 | 32 | 32 | 32 | 32 |
| p | <0.001 | <0.001 | <0.001 | <0.001 | <0.001 |



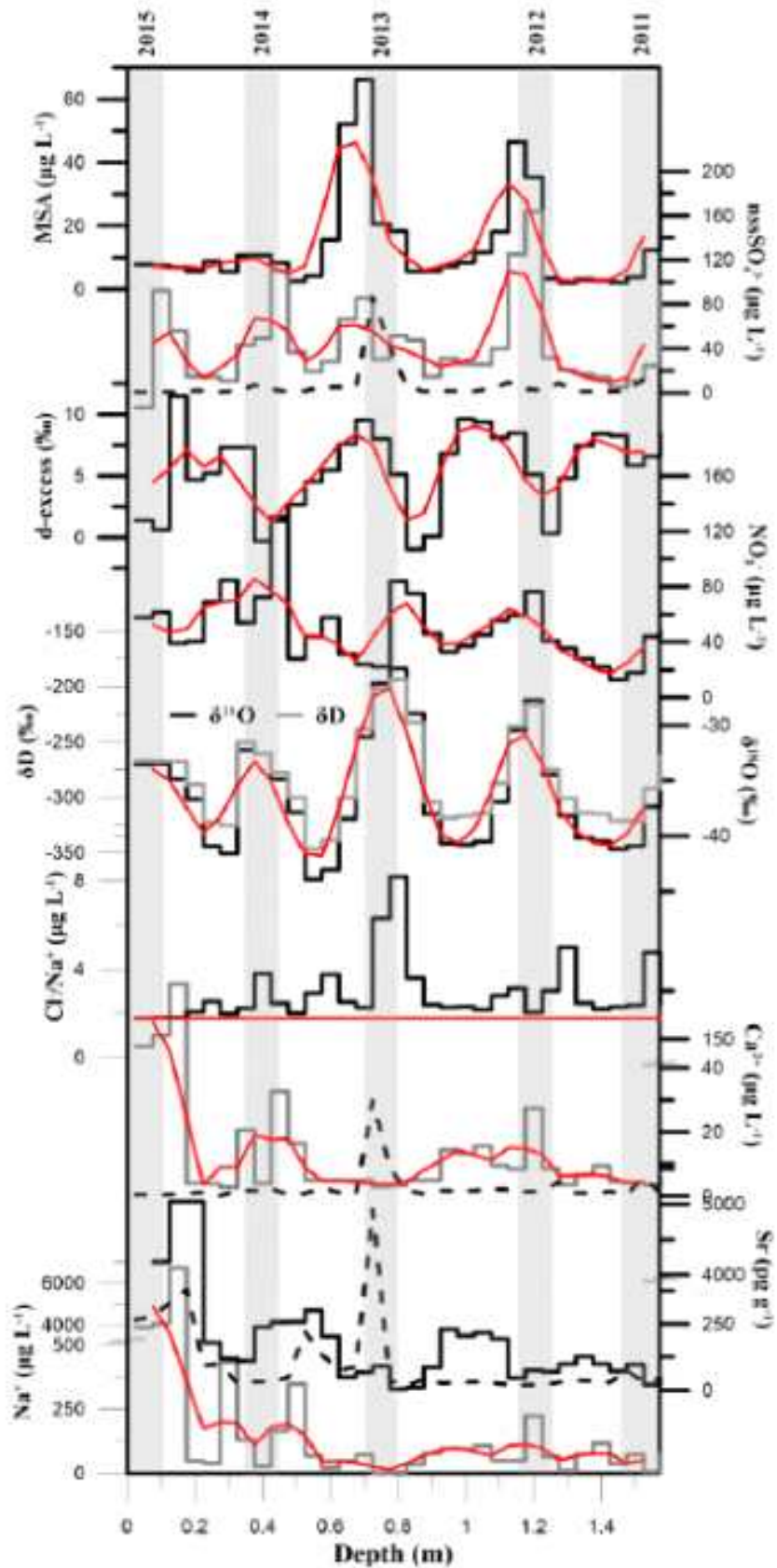


Fig 3.2.1. Concentration vs. the depth profiles of isotopic composition and ionic species with 3-point running average (red lines). Cl/Na^+ ratio was shown with their typical seawater ratio of 1.794 (red line). The shaded area represents the summer peak from January 2011 to January 2015. Dashed lines (black) are the sea salt EF for SO_4^{2-} and Ca^{2+} and crustal EF for Sr which are highlights the sharp increase in January 2013.

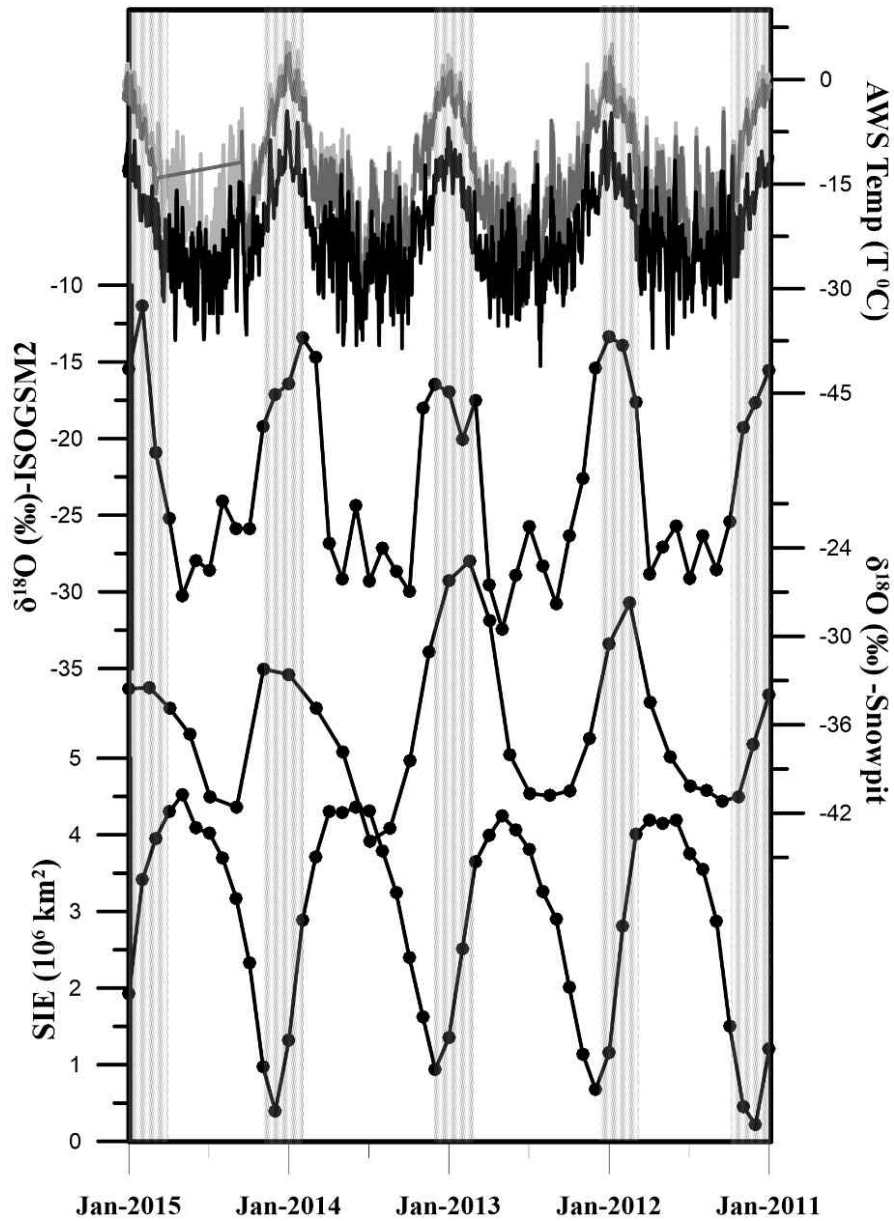


Fig 3.2.2. Comparison of monthly mean SIE in the Ross Sea, $\delta^{18}\text{O}$ of the snowpit and IsoGSM2 simulation, and daily temperature from Lola (bold black), Alessandra (black), and Eneide (grey).

Table 3.2.4. Annual mean values of $\delta^{18}\text{O}$, temperatures (temp) from AWS (Lola, Eneide, Alessandra) and ERA-Interim reanalysis data, SIE, snow accumulation rate (SA) from the snowpit and ERA-Interim reanalysis data (the largest values are highlighted in bold).

| Year | $\delta^{18}\text{O}$ | Temp (Lola) | Temp (Eneide) | Temp (Alessandra) | Temp (ERA) | SA (ERA) | SA (Snowpit) | SIE (10^6 km^2) |
|------|-----------------------|---------------|---------------|-------------------|---------------|---------------|---------------|-----------------------------|
| 2014 | -36.05 | -22.30 | -13.32 | -10.19 | -29.07 | 137.88 | 129.85 | 3.01 |
| 2013 | -36.49 | -22.62 | -13.62 | -15.16 | -28.96 | 159.84 | 129.85 | 3.10 |
| 2012 | -35.16 | -22.54 | -13.60 | -15.33 | -28.53 | 162.15 | 148.40 | 2.78 |
| 2011 | -37.16 | -21.44 | -12.48 | -14.04 | -27.14 | 203.74 | 166.95 | 2.74 |

Snow-Pit Record from a Coastal Antarctic Site and Its Preservation of Meteorological Features

YALALT NYAMGEREL,^{a,b} SANG-BUM HONG,^b YEONGCHEOL HAN,^b SONGYI KIM,^{a,b} JEONGHOON LEE,^a
AND SOON DO HUR^b

^a Department of Science Education, Ewha Womans University, Seoul, South Korea

^b Division of Glacial Environment Research, Korea Polar Research Institute, Incheon, South Korea

(Manuscript received 22 September 2020, in final form 19 May 2021)

ABSTRACT: Polar snow pits or ice cores preserve valuable information derived from the atmosphere on past climate and environment changes. A 1.57-m snow-pit record from the coastal site (Styx Glacier) in eastern Antarctica covering the period from January 2011 to January 2015 was discussed and compared with meteorological variables. The dominant contribution of the deposition of sea-salt aerosols due to the proximity of the site to the ocean and processes of sea ice formation was revealed in the ionic concentrations. Consistent seasonal peaks in $\delta^{18}\text{O}$, δD , MSA, nssSO_4^{2-} , and NO_3^- indicate the strong enhancement of their source during warm periods, whereas the sea-salt ions (Na^+ , K^+ , Mg^{2+} , Ca^{2+} , Cl^- , and totSO_4^{2-}) exhibit a distinct distribution. Monthly mean $\delta^{18}\text{O}$ positively correlates with the air temperature record from an automatic weather station (AWS) located in the main wind direction. Despite the shortness of the record, we suspect that the slight depletion of the isotopic composition and lowering of the snow accumulation could be related to the cooler air temperature with the decrease of open sea area. Consistency with previous studies and the positive correlation of sea-salt ions in the snow pit indicate the relatively good preservation of snow layers with noticeable climate and environmental signals [e.g., changes in sea ice extent (SIE) or sea surface temperature]. We report a new snow-pit record, which would be comparative and supportive to understand similar signals preserved in deeper ice cores in this location.

KEYWORDS: Antarctica; Sea ice; Snow

3.3. 장보고기지 주변 스노우핏의 화학성분, 동위원소성분의 계절성

장보고기지가 건설되기 전 획득했던 스노우핏 시료의 화학성분과 불안정동위원소를 분석하여 이들의 계절성을 이용하여 스노우핏의 연대를 추정하고 해안가 근처의 스노우핏시료의 특성을 파악하였다. 이는 2021년 Polish Polar Research에 출판되었다. 발췌된 내용을 아래에 제시하였다.

Information on the spatial and temporal variabilities of snow chemistry is crucial in glaciochemical studies (Dansgaard 1964; Jouzel and Masson-Delmotte 2010). However, obtaining reliable relationships between chemical and isotopic data and atmospheric composition is strongly dependent on the understanding of how changes in source intensity and transport efficiency can be stored in snow in different climatic conditions and how changes in the chemical and physical features of snow deposition, varying the depositional and post-depositional processes, affect the snow layer composition (Udisti *et al.* 1999; Stenni *et al.* 2000; Rhodes *et al.* 2012).

This study examined the four surface snow samples and 1.95-m-deep snowpit in the vicinity of the Jang Bogo Station in Antarctica. Seasonal variations of the isotopic and chemical compositions of snowpits can provide useful tools for dating the age of the snowpit and examining the sources of aerosol.

The isotopic and ionic compositions of the surface snow and snowpit were shown in table 3.1 and the vertical profiles shown in the figures 3.3–3.5. Distinct seasonal variations of stable water

isotopes of the snowpit were observed, with a slope of 8.2 from the linear isotopic relationship (figure 3.2) between oxygen and hydrogen, which indicates that the snow accumulated during three years without a significant post-depositional process. Based on the seasonal layers with dD and $d^{18}O$ maxima and minima, it was determined that the snowpit contained snow deposited over a three-year period (2008–2010). The positive correlations ($r > 0.85$) between sea-salt ions and the values of the MSA and $nssSO_4^{2-}$ warm period indicate the contribution of an oceanic source. This study will support further investigations in this region.

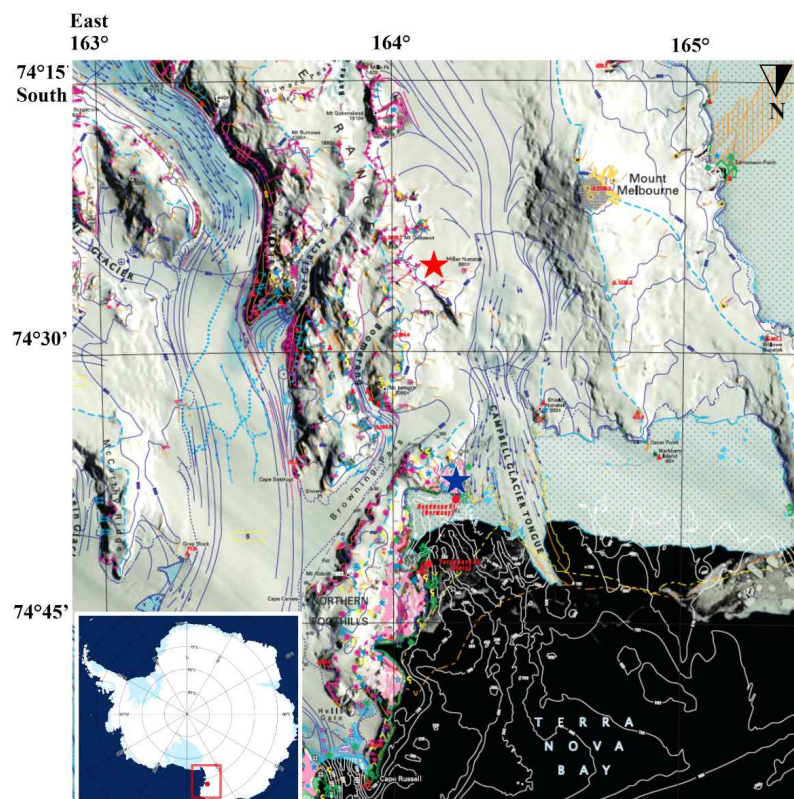


Fig 3.3.1. Location of the snowpit (red star) near the Korean Jang Bogo Station (blue star) in Terra Nova Bay, East Antarctica.

Table 3.3.1. The isotopic and chemical compositions of four snow samples (JBG-01, JBG-01, JBG-03, JBG-04) and snowpit.

| | JBG-01 | JBG-02 | JBG-03 | JBG-04 | Snowpit mean | Snowpit SD* |
|-------------------------------|---|---|---|---|-------------------------------|-------------|
| Location | S74° 36.665' E164° 13.536' North of JBS | S74° 37.097' E164° 12.239' Northwest of JBS | S74° 37.249' E164° 11.644' Northwest of JBS | S74° 37.489' E164° 12.894' Southwest of JBS | S74° 25.344' E164° 10.429' | |
| MSA | 47.88 | 522.62 | 494.68 | 504.28 | 36.59 | 32.54 |
| Cl ⁻ | 759.21 | 15,329.19 | 10,997.50 | 20,394.78 | 493.51 | 546.08 |
| SO ₄ ²⁻ | 212.73 | 2614.34 | 2085.81 | 3166.07 | 205.70 | 116.18 |
| NO ₃ ⁻ | 189.08 | 1582.84 | 1469.41 | 1587.28 | 64.24 | 78.81 |
| Na ⁺ | 412.45 | 8674.51 | 6406.89 | 11,635.68 | 298.32 | 312.94 |
| K ⁺ | 70.43 | 582.13 | 565.36 | 376.85 | 22.32 | 18.95 |
| Mg ²⁺ | 175.86 | 2160.94 | 1916.33 | 2495.20 | 56.05 | 68.89 |

| | | | | | | |
|-------------------|--------|---------|---------|---------|---------|-------|
| Ca ²⁺ | 74.94 | 3262.69 | 3078.66 | 3248.20 | 51.64 | 71.95 |
| d ¹⁸ O | -13.88 | -14.86 | -18.15 | -16.77 | -24.34 | 4.84 |
| dD | -99.48 | -117.88 | -146.55 | -130.79 | -186.50 | 39.82 |
| d-excess | 11.57 | 0.98 | -1.36 | 3.35 | 8.22 | 5.16 |

Note: SD: standard deviation.

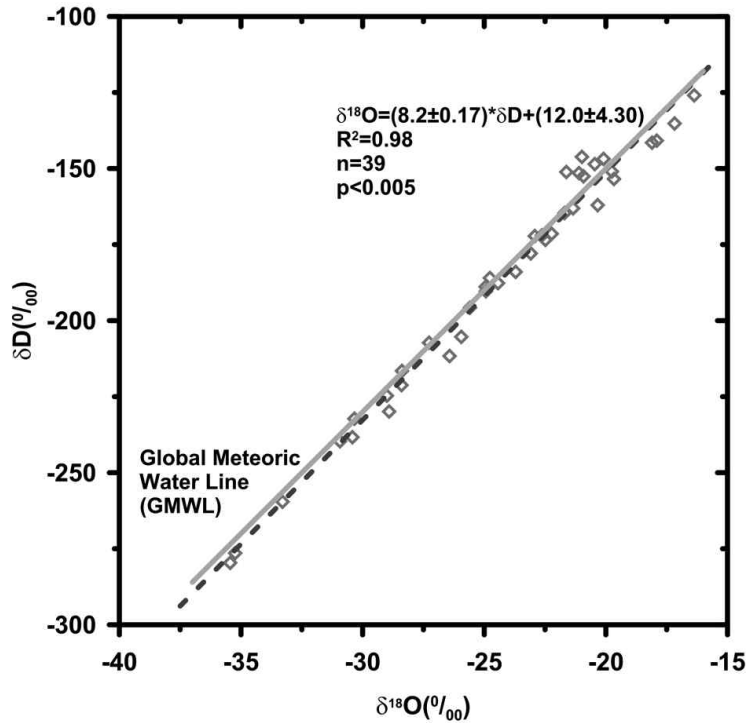


Fig 3.3.2. The linear regression line between dD and d¹⁸O. The regression line is similar to that of the GMWL (grey line) and LMWL.

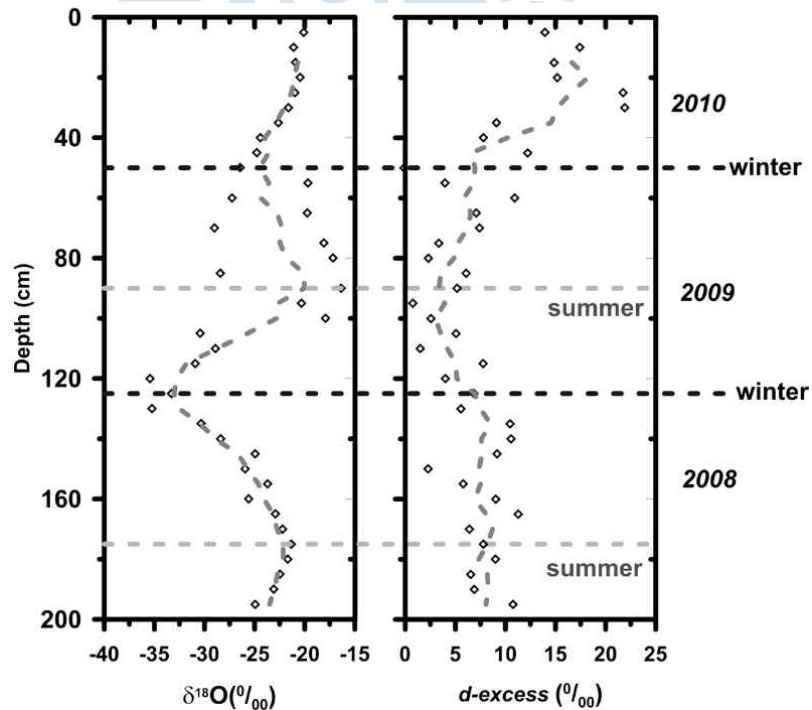


Fig 3.3.3. Vertical profiles of stable water isotopes. Summer and winter in the snowpit were defined from the maximum and minimum values of the stable water isotopes, respectively.

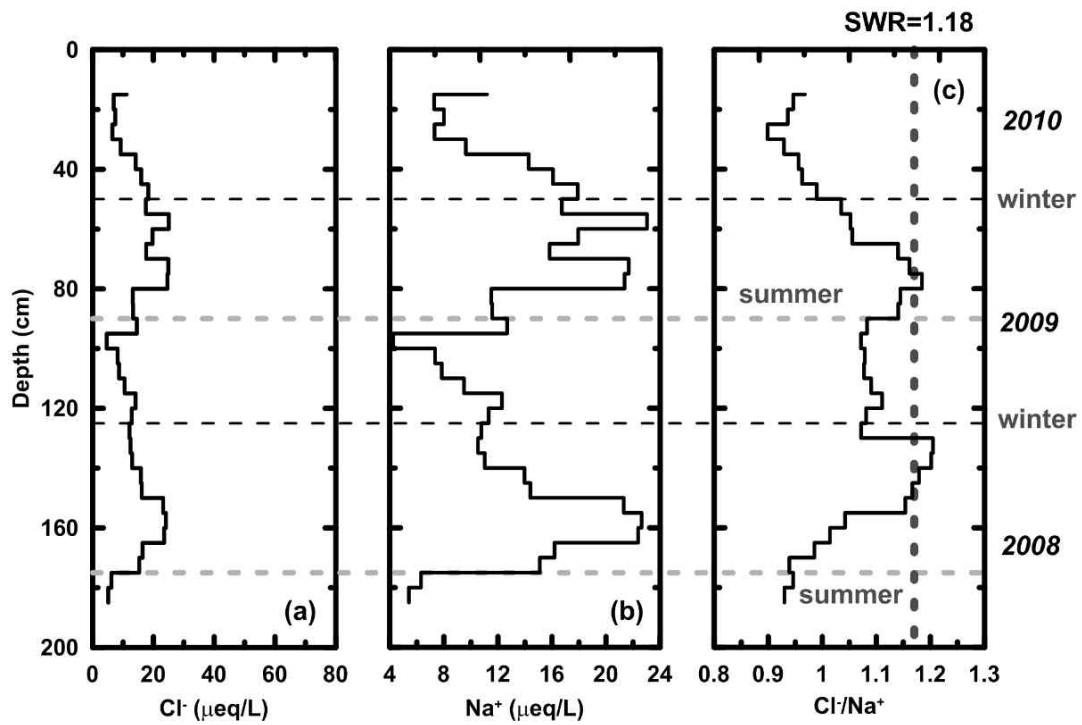


Fig 3.3.4. Vertical profiles of Cl^- , Na^+ , and the Cl^-/Na^+ ratio. The dashed line represents the Cl^-/Na^+ ratio in the Sea Water Ratio (SWR, 1.18).

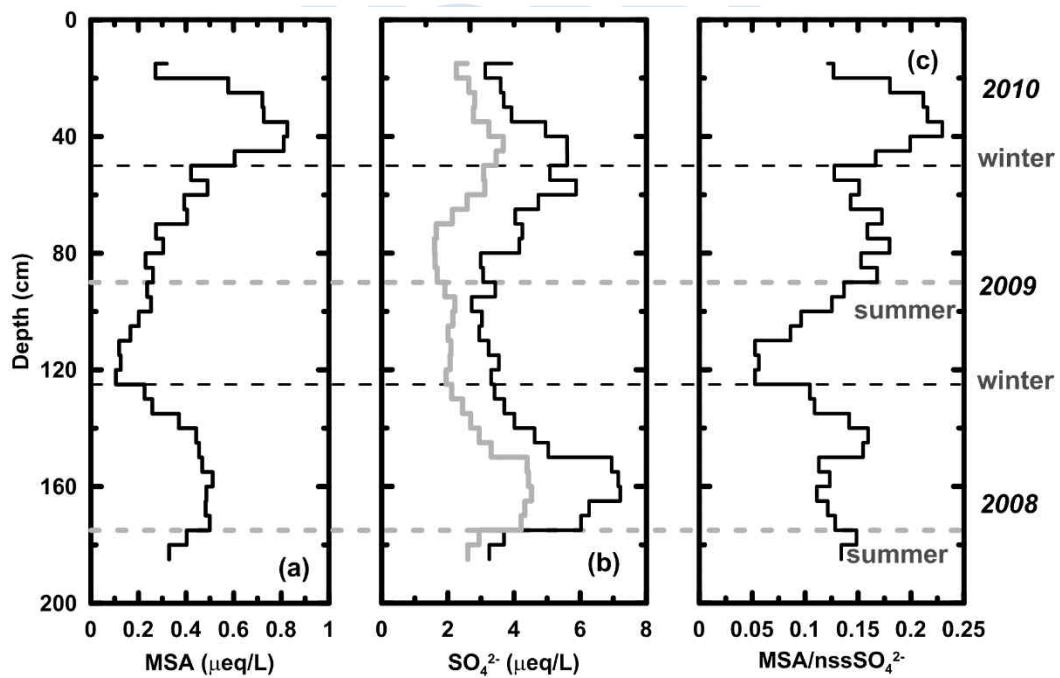


Fig 3.3.5. Vertical profiles of MSA, sulfate, and $\text{MSA}/\text{nssSO}_4^{2-}$ ratio. The gray line in the middle indicates non-sea-salt (nss).



Seasonality of isotopic and chemical composition of snowpack in the vicinity of Jang Bogo Station, East Antarctica

Soon Do HUR¹ , Jiwoong CHUNG¹ , Yalalt NAMGEREL^{1,2} 
and Jeonghoon LEE^{2,*} 

¹Division of Glacial Environment Research, Korea Polar Research Institute,
26, Songdomirae-ro, Yeonsu-gu, Incheon 21990, Korea
<sdhur@kopri.re.kr> <jjw79@kopri.re.kr> <yalalt@gmail.com>

²Department of Science Education, Ewha Womans University, 52, Ewhayeodae-gil,
Seodaemun-gu, Seoul 120-750, Korea

* *corresponding author* <jeonghoon.d.lee@gmail.com>

극지연구소

3.4. 물순환에서 ^{17}O 의 적용가능성에 대한 리뷰

^{17}O 를 분석하고 이를 이용하여 극지역에서 어떻게 활용할 수 있는가에 대한 조사를 수행하였으며, 특히 ^{17}O 의 과잉값을 이용하여 남극 연구에 어떻게 활용할 수 있는가에 대한 자료를 제시하였다. 본 논문은 molecules에 출판되었다.

The triple oxygen isotopes (^{16}O , ^{17}O , and ^{18}O) are very useful in hydrological and climatological studies because of their sensitivity to environmental conditions. This review presents an overview of the published literature on the potential applications of ^{17}O in hydrological studies which provides information on atmospheric conditions at the moisture source and isotopic fractionations during transport and deposition processes. This study summarized the range of $\delta^{18}\text{O}$, λ_{ref} and ^{17}O -excess in the published studies (table 4.1).

The variations of $\delta^{17}\text{O}$ from the developed global meteoric water line, with a slope of 0.528, indicate the importance of regional or local effects on the ^{17}O distribution. In polar regions, factors such as the supersaturation effect, intrusion of stratospheric vapor, post-depositional processes (local moisture recycling through sublimation), regional circulation patterns, sea ice concentration and local meteorological conditions determine the distribution of ^{17}O -excess. Numerous studies have used these isotopes to detect the changes in the moisture source, mixing of different water vapor, evaporative loss in dry regions, re-evaporation of rain drops during warm precipitation and convective storms in low and mid-latitude waters. Owing to the large variation of the spatial scale of hydrological processes with their extent (i.e., whether the processes are local or regional), more studies based on isotopic composition of surface and subsurface water, convective precipitation, and water vapor, are required. In particular, in situ measurements are important for accurate simulations of atmospheric hydrological cycles by isotope-enabled general circulation models.

Table 3.4.1. Summary of published $\delta^{18}\text{O}$, λ_{ref} and ^{17}O -excess in different samples. All values are averaged from published values. We note that the sampling location, period, and sampling numbers are distinct depending on the studies; thus, values are representative of local scale variations

| Sample Type | $\delta^{18}\text{O}$ Range | ^{17}O -Excess Mean or Range (per meg) | λ_{ref} | Analytical Method | Time Scale | Reference |
|--|---------------------------------|---|------------------------|----------------------|--|-----------------------|
| Low- and mid-latitude Precipitation | | | | | | |
| Vapor (Mt.Zugspitze, Germany) | (-34.4 to -20.4) | (30 to 82) | 0.5265 | IRMS | 2016 (Feb to May) | Surma et al., 2021 |
| Cave water (Canada and USA) | -9.69 (-17.67 to -6.39) | 0.05 (0.03 to 0.07) | 0.530 | IRMS | 2005 (Feb, Jul) | Luz et al., 2010 |
| Cave drip waters (Northwest Switzerland) | -8.7 | 19 | - | Picarro CRDS | 2010 (Nov) to 2014 (Jun) | Affolter et al., 2015 |
| Fluid inclusions (Northwest Switzerland) | -8.3 | 10 | - | Picarro CRDS | 2012 (Mar) to 2014 (Jun) | Affolter et al., 2015 |
| Leaf water (Mpala central Kenya) | 7.84 (-0.27 to 16.14) | -0.06 (-0.16 to 0.04) | - | IRMS | 2012 (Jun-Jul) | Li et al., 2017 |
| Stem water (Mpala central Kenya) | -2.46 (-4.71 to 0.59) | 0.02 (0.01 to 0.03) | - | IRMS | 2012 (Jun-Jul) | Li et al., 2017 |
| Pond (Sistan Oasis, Iran) | 25.83 (13.81 to 29.07) | -144.4 (-172 to -56) | - | IRMS | - | Surma et al., 2015 |
| Lake and pond | -8.06 (-16.03 to 4.19) | 0.02 (-0.02 to 0.04) | 0.528 | IRMS | 2002, 2008 | Luz et al., 2010 |
| Surface water | -8.88 (-20.31 to 9.56) | -46.4 to 55.67 (mostly 14 to 33) | 0.528 | IRMS | Global scale | Aron et al., 2020 |
| River, terminal lakes, well, spring, irrigation channel (Sistan Oasis, Iran) | -1.69 (-6.84 to 14.03) | -3.91 (-59 to 25) | - | IRMS | - | Surma et al., 2015 |
| Lake and river (western USA) | -9.58 (-19.11 to -0.34) | 5.28 (-39 to 46) | - | IRMS | - | Passey et al., 2019 |
| Dam water (Mpala central Kenya) | -1.08 (-3.98 to 2.26) | 0.01 (-0.004 to 0.02) | - | IRMS | 2012 (Jun-Jul) | Li et al., 2017 |
| Tap, spring water (Israel) | -4.99 (-5.74 to -4.24) | 0.04 (0.03 to 0.05) | 0.515 | IRMS | 2008 | Luz et al., 2010 |
| Tap water (continental USA) | -8 ± 4.7 (-20.7 to -0.7) | 17 ± 11 (-6 to 43) | 0.526 to 0.527 | IRMS | 2006 to 2011 | Li et al., 2015 |
| Tap and puddle water (Mpala central Kenya) | 3.36 (2.33 to 4.39) | -0.01 (-0.01 to -0.003) | - | IRMS | 2012 (Jun-Jul) | Li et al., 2017 |
| Precipitation (Northwest Switzerland) | -9.9 | 18 | - | Picarro CRDS | 2012 (Mar) to 2014 (Jun) | Affolter et al., 2015 |
| Precipitation (Okinawa Island, Japan) | -4.81 (-9.88 to -1.05) | 25.26 (4 to 54) | - | Picarro CRDS | 2011 (Jan) to 2012 (Dec) | Uechi et al., 2019 |
| Precipitation (central USA) | -6.25 | 31 | 0.5275 | OA-ICOS | 2014 (Jun) to 2018 (May) | Tian et al., 2019 |
| Rain (Indonesia, India, and Israel) | -5.45 (-9.03 to -2.53) | 0.04 (0.02 to 0.06) | 0.522 | IRMS | 2005 (Mar to Nov) 2001 to 2008 2008 (Feb to Aug) | Luz et al., 2010 |
| Water vapor (south Indian and Southern Ocean) | -15.45 (-23.41 to -11.65) | 13.51 (-6 to 46) | 0.532 | IRMS | 2005 (Dec) to 2006 (Jan) | Uemura et al., 2010 |
| Seawater (Atlantic, Pacific Ocean, Mediterranean, and Northern Red Sea) | 0.42 (-0.42 to 2.43) | -0.0045 (-0.01 to 0.0038) | 0.528 | IRMS | - | Luz et al., 2010 |
| Snow (Mt.Zugspitze, Germany) | (-21.7 to -8.3) | (17 to 62) | - | IRMS | - | Surma et al., 2021 |

| | | | | | | |
|--|------------------------------|-------------------------|--------|------|-----------------------------|-----------------------------|
| Snow, ice (Canada, Montenegro) | -17.34 (-26.11 to -5.44) | 0.02 (-0.01 to 0.04) | 0.529 | IRMS | 2009, 2010 | Luz et al., 2010 |
| High-latitude precipitation | | | | | | |
| Vapor (NEEM, Greenland) | -41.77 (-44.63 to -38.33) | 32.33 (15 to 48) | 0.528 | IRMS | 2008 (Aug) | Landais et al., 2012a |
| Snow precipitation (NEEM, Greenland) | -29.60 (-35.53 to -24.33) | 35.67 (23 to 43) | - | IRMS | 2008 (Aug) | Landais et al., 2012a |
| Firn core (NEEM, Greenland) | -32.17 (-38.80 to -26.70) | 49.70 (30 to 73) | - | IRMS | 2003 (Jan) to 2005 (Aug) | Landais et al., 2012a |
| Snow pit (Vostok) | -57.13 (-61.20 to -51.39) | 7.43 (-36 to 42) | - | IRMS | 1949 to 2008 | Winkler et al., 2013 |
| Surface snow (traverse from Zhongshan station to Dome A) | -34.30 (-58.69 to -17.60) | 34.95 (9 to 51) | - | IRMS | 2009 (Dec) to 2010 (Jan) | Pang et al., 2015 |
| Snow (transect from Syowa to Dome Fuji) | -47.26 (-56.69 to -30.20) | 24.82 (6.1 to 43.8) | - | IRMS | - | Touze et al., 2016 |
| Ice core (Vostok) | -58 (-50.74 to -62.05) | 24.31 (-6 to 54) | - | IRMS | 150ka years | Landais et al., 2008 |
| Surface snow (Vostok, Antarctica) | -41.27 (-28.23 to -51.03) | 44.5 (25 to 62) | 0.528 | IRMS | - | Landais et al., 2008 |
| Snow or ice (Dome F, Antarctica) | -58.42 | -0.006 | - | IRMS | - | Luz et al., 2010 |
| Ice core (Talos Dome, Antarctica) | -41.67 to -36.52 | - | 0.5278 | IRMS | 9.15 to 33.78 ka age | Winkler et al., 2012 |
| Ice core (WAIS, Antarctica) | -35.44 (-42.68 to -31.61) | 25.22 (2.9 to 38.46) | - | IRMS | 25 ka | Schoenemann et al., 2019 |
| Ice core (Taylor Dome, Antarctica) | -39.56 (-42.92 to -37.36) | 14.28 (-1 to 28) | 0.5313 | IRMS | - | Schoenemann et al., 2019 |
| Ice core (Siple Dome Antarctica) | -31.31 (-36.21 to -24.02) | 19 (8 to 27) | - | IRMS | - | Schoenemann et al., 2019 |
| Snow precipitation (Vostok, Antarctica) | -68.47 to -50.51 | -27 to 29 | 0.5308 | IRMS | 2000 (Feb-Oct) | Landais et al., 2012b |
| Snow precipitation (Vostok, Antarctica) | -58.5 to -52.6 | - | 0.5269 | IRMS | 1999 (Dec) to 2000 (Jun) | Touze et al., 2016 |
| Ice core (Dome C, Antarctica) | -56.48 to -46.639 | - | 0.5294 | IRMS | 7.61-24.8 ka age | Winkler et al., 2012 |
| Snow precipitation (Dome C, Antarctica) | -55.58 (-69.63 to -38.89) | 18.43 (-11 to 47) | 0.5282 | IRMS | 2010 (Sep-Nov) | Touze et al., 2016 |
| Snow (Dome C, Antarctica) | -54.25 (-61.35 to -48.19) | 31.64 (14 to 47) | 0.5287 | IRMS | 2010 (Dec) to 2011 (Dec) | Touze et al., 2016 |
| Snow pit (Dome C, Antarctica) | -51.14 (-55.31 to -46.06) | 31.68 (17 to 51) | 0.528 | IRMS | - | Touze et al., 2016 |

Review

Review on Applications of ^{17}O in Hydrological Cycle

Yalalt Nyamgerel ¹, Yeongcheol Han ², Minji Kim ¹, Dongchan Koh ³ and Jeonghoon Lee ^{1,*}

¹ Department of Science Education (Earth Sciences), Ewha Womans University, Seoul 03760, Korea; yalalt@gmail.com (Y.N.); minji.jane.kim@gmail.com (M.K.)

² Korea Polar Research Institute, Incheon 21990, Korea; yhan@kopri.re.kr

³ Korea Institute of Geoscience and mineral Resources, Daejeon 34132, Korea; chankoh@kigam.re.kr

* Correspondence: jeonghoon.d.lee@gmail.com; Tel.: +82-2-3277-3794

Abstract: The triple oxygen isotopes (^{16}O , ^{17}O , and ^{18}O) are very useful in hydrological and climatological studies because of their sensitivity to environmental conditions. This review presents an overview of the published literature on the potential applications of ^{17}O in hydrological studies. Dual-inlet isotope ratio mass spectrometry and laser absorption spectroscopy have been used to measure ^{17}O , which provides information on atmospheric conditions at the moisture source and isotopic fractionations during transport and deposition processes. The variations of $\delta^{17}\text{O}$ from the developed global meteoric water line, with a slope of 0.528, indicate the importance of regional or local effects on the ^{17}O distribution. In polar regions, factors such as the supersaturation effect, intrusion of stratospheric vapor, post-depositional processes (local moisture recycling through sublimation), regional circulation patterns, sea ice concentration and local meteorological conditions determine the distribution of ^{17}O -excess. Numerous studies have used these isotopes to detect the changes in the moisture source, mixing of different water vapor, evaporative loss in dry regions, re-evaporation of rain drops during warm precipitation and convective storms in low and mid-latitude waters. Owing to the large variation of the spatial scale of hydrological processes with their extent (i.e., whether the processes are local or regional), more studies based on isotopic composition of surface and subsurface water, convective precipitation, and water vapor, are required. In particular, in situ measurements are important for accurate simulations of atmospheric hydrological cycles by isotope-enabled general circulation models.

Keywords: ^{17}O -excess; kinetic fractionation; stable water isotopes



Citation: Nyamgerel, Y.; Han, Y.; Kim, M.; Koh, D.; Lee, J. Review on Applications of ^{17}O in Hydrological Cycle. *Molecules* **2021**, *26*, 4468. <https://doi.org/10.3390/molecules26154468>

3.5. 희토류원소의 지하수 및 빙하연구에서의 의미

지하수에서 희토류 원소는 암석과의 반응으로 지하수로 이동하게 되며, 풍화로 인해 발생한 먼지 등에 의해 빙하시료에 희토류원소가 남게 된다. 따라서, 빙하에서의 희토류원소의 특성은 주변 지질에 의해 결정되며, 이를 통해 대기순환을 지시할 수 있게 된다. 본 내용은 한국지구과학회지에 영문판으로 출판되었다.

Several publications concerned with rare earth element behavior and /or distribution have been reviewed in order to determine geochemical processes that likely exert controls on the REE concentrations and fractionation patterns in groundwaters and to test whether these elements can be useful tracers of groundwater-rock interaction and groundwater flow paths in small size catchments. An ICP-MS (Inductively Coupled Plasma Mass Spectrometry), equipped with an ultrasonic nebulizer and active-film multiplier detector, has been used to attempt to determine rare earth elements directly in groundwater. As a consequence there have now been an increasing number of studies dedicated to the geochemistry of dissolved

REE. This review focuses on distribution of rare earth elements in groundwater and rare earth elements as groundwater geochemistry tracers. In the end, REE is depicted as a geochemical tool for ice core study to track source regions of particles.

| | |
|--|---|
| J. Korean Earth Sci. Soc., v. 42, no. 4, p. 383–389, August 2021 https://doi.org/10.5467/JKESS.2021.42.4.383 | ISSN 1225-6692 (printed edition) ISSN 2287-4518 (electronic edition) |
| Distribution of Rare Earth Elements and Their Applications as Tracers for Groundwater Geochemistry - A Review | |
| Heejin Hwang¹, Yalalt Nyamgerel², and Jeonghoon Lee^{2,*} | |
| ¹ Korea Polar Research Institute, Incheon 21990, Korea ² Department of Science Education, Ewha Womans University, Seoul 03760, Korea | |
| Abstract: Several studies investigating the behavior and environmental distribution of rare earth elements (REEs) have been reviewed to determine the geochemical processes that may affect their concentrations and fractionation patterns in groundwater and whether these elements can be used as tracers for groundwater-rock interactions and groundwater flow paths in small catchments. Inductively coupled plasma-mass spectrometry (ICP-MS), equipped with an ultrasonic nebulizer and active-film multiplier detector, is routinely used as an analytical technique to measure REEs in groundwater, facilitating the analysis of dissolved REE geochemistry. This review focuses on the distribution of REEs in groundwater and their application as tracers for groundwater geochemistry. Our review of existing literature suggests that REEs in ice cores can be used as effective tracers for atmospheric particles, aiding the identification of source regions. | |
| Keywords: rare earth element, groundwater-rock interaction, groundwater flow paths, ice core study | |

3.6. 높은 강설량을 나타내고 있는 아문젠 지역의 스노우핏

아문젠 해역 주변은 최근 급격한 빙하의 용융으로 인해 많은 주목을 받고 있는 지역이다. 따라서, 빙하의 질량변화가 중요한 지역이며, 강설량을 복원하는 것이 이 지역에서 고기후 및 대기 모델링에 중요한 변수를 측정하는 일이 될 것이다. 본 연구는 2.5미터의 스노우핏의 화학성분 및 동위원소성분을 분석하여 해안지역에서 높은 강설량을 보고하는 연구이다. 현재 Polish Polar Research에 투고 중이다.

Polar snow and its accumulation preserve valuable information derived from atmosphere on past climate and environment changes in favorable resolution particularly in coastal sites. Amundsen Sea sector of West Antarctica is known as a critical site related to the ice losing from coastal ice shelves due to the intrusion of circumpolar deep water coupling with variabilities in regional winds (Dinniman *et al.* 2012, Mouginit *et al.* 2014). Ice coring in coastal Antarctic areas have been rising in recent years in the context of ice-ocean-atmospheric interaction (Mulvaney *et al.* 2021; Neff, 2020). Particularly, the region closer or center (coasts of Amundsen and Bellingshausen Sea) to the warming and melting spot is recommended for additional records (Steig and Neff, 2018).

A site-based information and evaluation of isotopic and chemical compositions are significant to examine the present-day snow compositions and its differences at regional and/or local scales and applications to the interpretation of the paleoclimate records (Stenni *et al.* 2000; Tuohy *et al.* 2015; Stenni *et al.* 2017). Thus, there is a need to improve site-based data to refine the interpretation of paleoclimate record due to significant spatial and temporal variabilities in snow accumulation and air

temperature (Masson-Delmotte *et al.* 2008) and the sparse instrumental data (Stenni *et al.* 2000; Tuohy *et al.* 2015). This study aims to characterize the isotopic and ionic compositions of snow deposited in seashore near to Amundsen Sea. High snow accumulation in the coastal site allows more high-resolution information in the chemical and isotopic compositions in the snowpit. The statistical summary and the correlation matrix for the snowpit shown in table 6.1 and 6.2. Decreasing trend in the snow layer as depth increases (Figure 2) and the increasing depth (Figure 3) were shown. The vertical profiles of the isotopes and ions were shown in figures 6.4, 6.6, and 6.7. Figure 6.5 show the meteorological parameters in the period corresponding to the snowpit age.

A 2.5-m deep snowpit excavated from the coastal ice rise (Moore Dome) near Amundsen Sea region in Feb 2012. THigh snow accumulation was detected in this site based on the seasonal variations of the MSA, nssSO_4^{2-} together with d^{18}O , dD , d -excess. Relatively warm and varied meteorological condition in austral winter in 2011 was traceable in the variations of $\delta^{18}\text{O}$, δD , and d -excess. This study state that the high snow accumulation in this site would allow sub-annual variations in climatological and environmental changes in longer ice cores from this location.

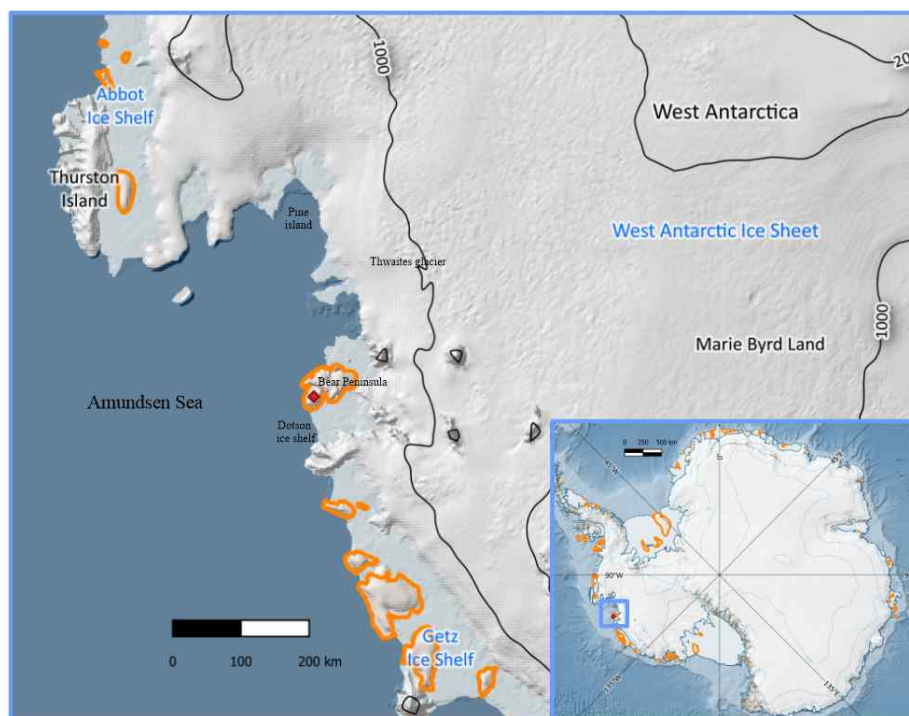


Fig 3.6.1. Location of a snowpit (red rhombus symbol) at Moore Dome ice rise in Bear Peninsula, West Antarctica. Ice rises (colored in yellow) are shown, and the map is generated by the Quantarctica GIS package.

Table 3.6.1. Mean, standard deviation, minimum, maximum values of isotope (‰) and ions ($\mu\text{eq/L}$).

| <i>Variables</i> | Mean | Standard Deviation | Minimum | Maximum |
|-----------------------|-------------|---------------------------|----------------|----------------|
| δD | -107.11 | 21.97 | -156.65 | -70.96 |
| $\delta^{18}\text{O}$ | -14.05 | 2.83 | -20.85 | -9.03 |
| d -excess | 5.27 | 3.05 | 0.25 | 11.76 |

| | | | | |
|----------------------------------|-------|-------|-------|-------|
| Na ⁺ | 9.31 | 9.65 | 0.27 | 64.95 |
| NH ₄ ⁺ | 0.25 | 0.13 | 0.06 | 0.57 |
| K ⁺ | 0.21 | 0.25 | 0.00 | 1.57 |
| Mg ²⁺ | 2.20 | 2.15 | 0.26 | 14.00 |
| Ca ²⁺ | 0.52 | 0.43 | 0.07 | 2.40 |
| MSA | 0.40 | 0.45 | 0.01 | 1.68 |
| Cl ⁻ | 11.67 | 12.44 | 0.43 | 83.69 |
| SO ₄ ²⁻ | 1.88 | 1.61 | 0.19 | 7.69 |
| nssSO ₄ ²⁻ | 0.76 | 1.05 | -0.43 | 3.53 |
| NO ₃ ⁻ | 0.47 | 0.37 | 0.07 | 1.86 |

Table 3.6.2. Correlation matrix for the isotopes and ions in the snowpit. Correlation coefficient values larger than 0.4 are underlined.

| | δD | $\delta^{18}O$ | <i>d-excess</i> | NO ₃ ⁻ | Cl ⁻ | SO ₄ ²⁻ | MSA | Na ⁺ | NH ₄ ⁺ | K ⁺ | Mg ²⁺ | Ca ²⁺ |
|-------------------------------|-------------|----------------|-----------------|------------------------------|-----------------|-------------------------------|------|-----------------|------------------------------|----------------|------------------|------------------|
| δD | 1.00 | | | | | | | | | | | |
| $\delta^{18}O$ | <u>0.99</u> | 1.00 | | | | | | | | | | |
| <i>d-excess</i> | -0.15 | -0.28 | 1.00 | | | | | | | | | |
| NO ₃ ⁻ | 0.09 | 0.02 | <u>0.51</u> | 1.00 | | | | | | | | |
| Cl ⁻ | -0.22 | -0.25 | 0.26 | 0.04 | 1.00 | | | | | | | |
| SO ₄ ²⁻ | -0.26 | -0.31 | <u>0.45</u> | 0.04 | <u>0.76</u> | 1.00 | | | | | | |
| MSA | -0.26 | -0.30 | 0.38 | -0.10 | 0.32 | <u>0.83</u> | 1.00 | | | | | |
| Na ⁺ | -0.21 | -0.24 | 0.27 | 0.05 | <u>1.00</u> | <u>0.76</u> | 0.32 | 1.00 | | | | |
| NH ₄ ⁺ | 0.18 | 0.12 | <u>0.45</u> | <u>0.50</u> | 0.35 | 0.56 | 0.42 | 0.36 | 1.00 | | | |
| K ⁺ | -0.19 | -0.22 | 0.27 | 0.08 | <u>0.99</u> | <u>0.74</u> | 0.30 | <u>0.99</u> | 0.39 | 1.00 | | |
| Mg ²⁺ | -0.23 | -0.26 | 0.28 | 0.05 | <u>1.00</u> | <u>0.77</u> | 0.34 | <u>1.00</u> | 0.37 | <u>0.99</u> | 1.00 | |
| Ca ²⁺ | -0.21 | -0.24 | 0.30 | 0.05 | <u>0.95</u> | <u>0.78</u> | 0.37 | <u>0.95</u> | <u>0.43</u> | <u>0.96</u> | <u>0.97</u> | 1.00 |

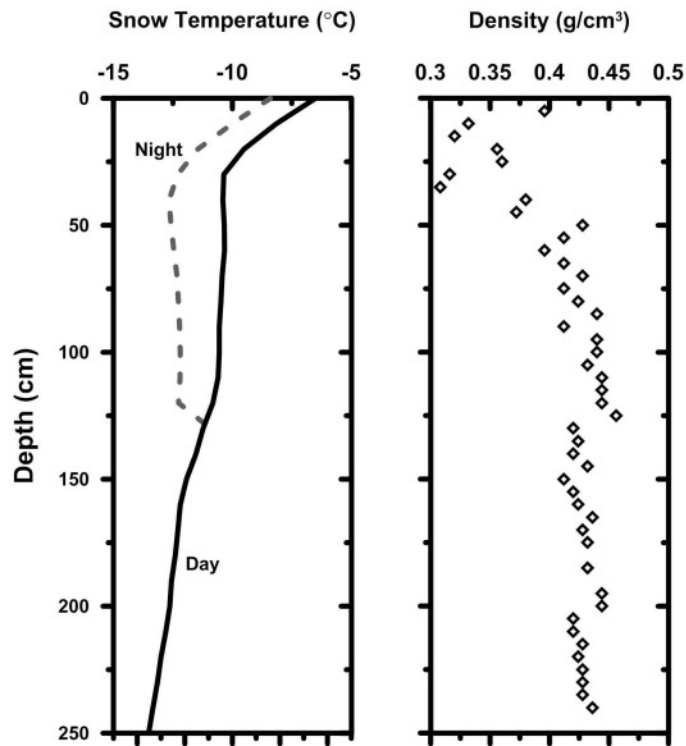


Fig 3.6.2. Vertical profiles of snow temperature and snow density in the Moore Dome snowpit

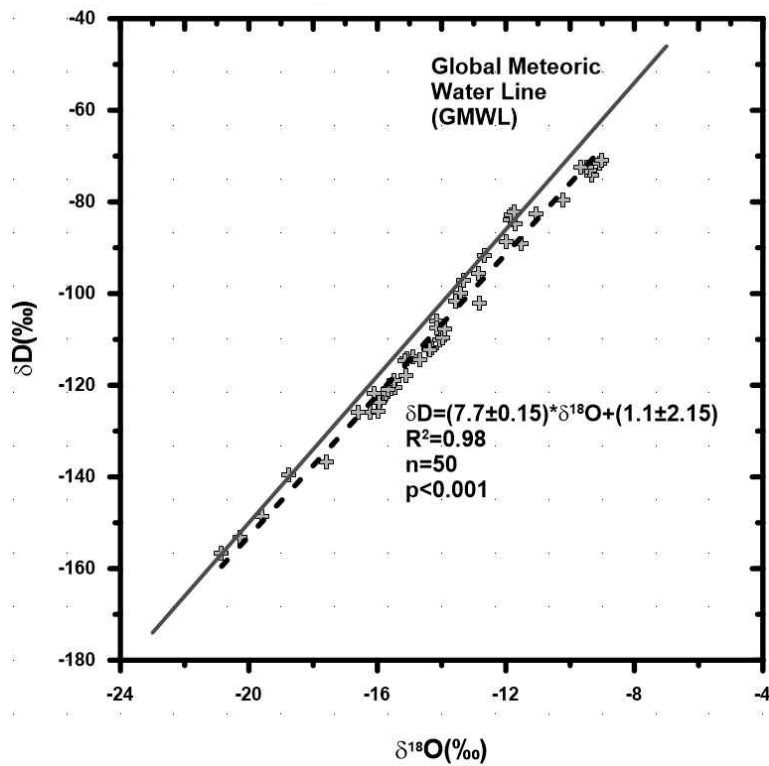


Fig 3.6.3. $\delta^{18}\text{O}$ - δD diagram of the snowpit with Global meteoric water line (Craig, 1961)

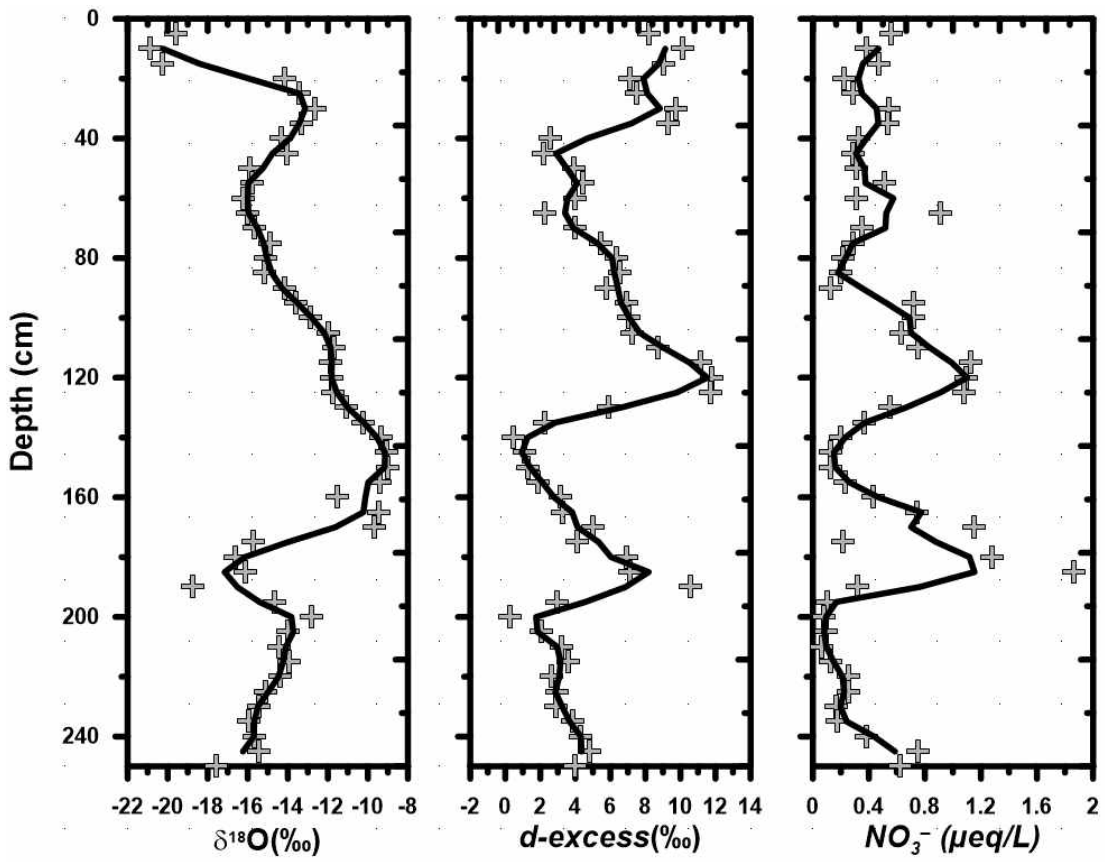
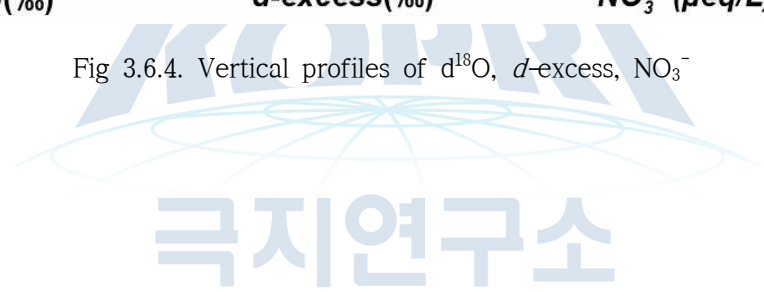


Fig 3.6.4. Vertical profiles of $d^{18}\text{O}$, $d\text{-excess}$, NO_3^-



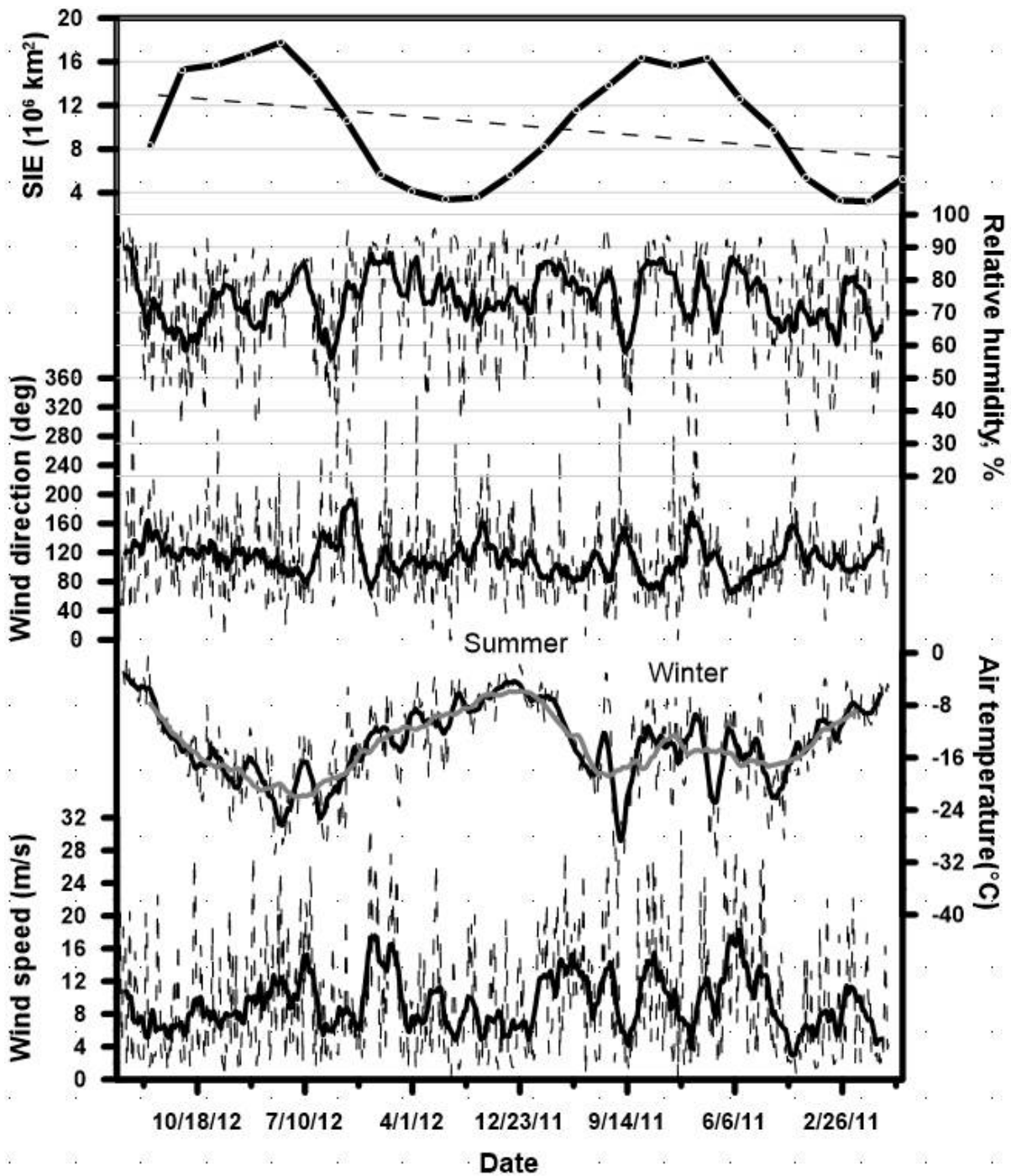


Fig 3.6.5. Daily mean and 15-point running averaged (grey line is 60 day-averaged for air temperature data only) meteorological data between Jan 2011 to Dec 2012 in Bear Peninsula AWS with monthly mean SIE data.

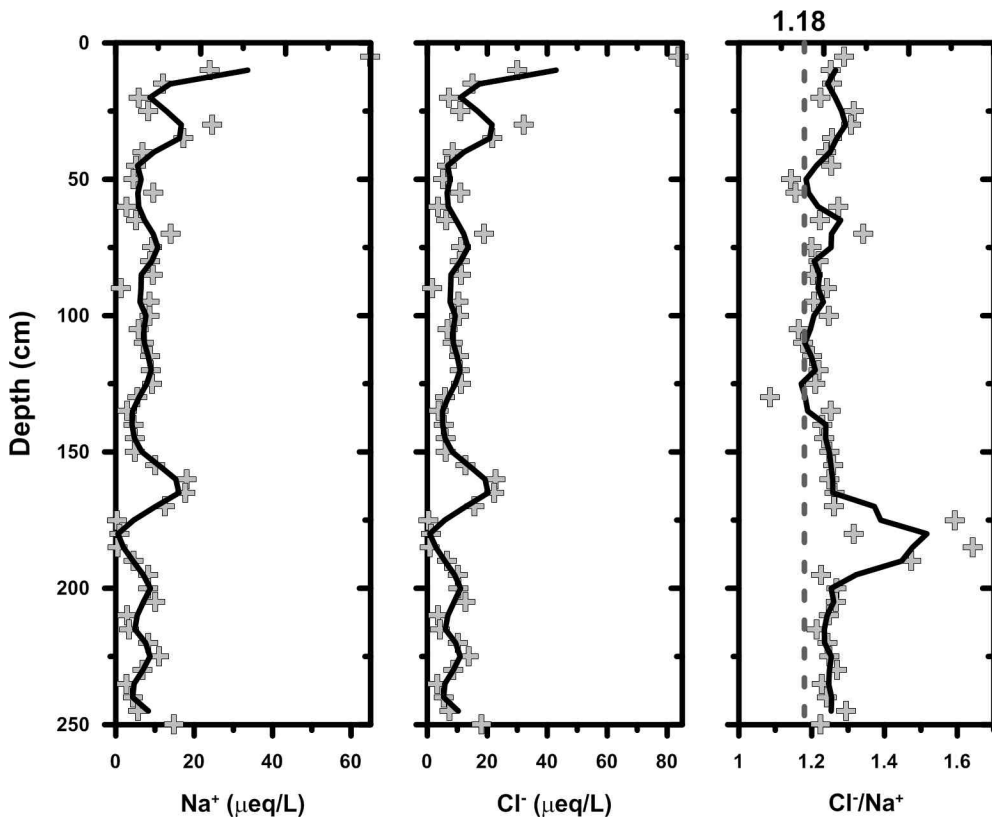


Fig 3.6.6. Vertical profiles of Na⁺ and Cl⁻ ions and their ratio

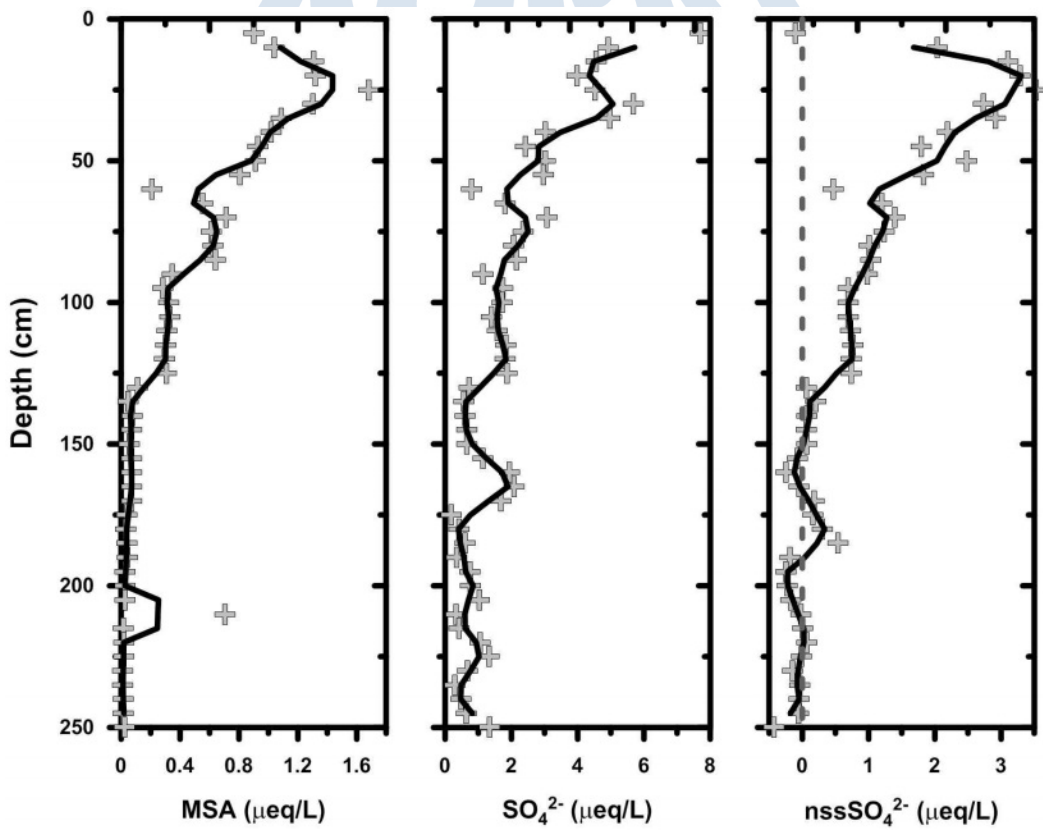


Fig 3.6.7. Vertical profiles of MSA, SO₄²⁻ and nssSO₄²⁻

**High snow accumulation observed by chemical and isotopic compositions
in a coastal ice rise in the Amundsen Sea, Antarctica**

By

Sang-Bum Hong¹, Yalalt Nyamgerel², Won Sang Lee¹ and Jeonghoon Lee^{2,*}

¹Division of Glacial Environmental Research, Korea Polar Research Institute, 26,
Songdomirae-ro, Yeonsu-gu, Incheon 21990, Korea
<hong909@kopri.re.kr> <wonsang@kopri.re.kr>

²Department of Science Education, Ewha Womans University, 52, Ewhayeodae-
gil, Seodaemun-gu, Seoul 120-750, Korea

<yalaltn@gmail.com> <jeonghoon.d.lee@gmail.com>

3.7. 얼음의 용해 시 이질성에 의한 물동위원소의 변화

얼음이 용해되면서 불안정동위원소 값은 주변 액체상의 물과 반응하면서 동위원소값에 변화가 발생하게 된다. 이는 갈수록 해안에서 주변에서 채취하는 빙하코어시료가 많아 지고 있는 상황에서 용융이 발생하게 되면 온도복원 등 물동위원소가 기후변화의 프록시로서의 정확도가 낮아지게 된다. 따라서, 얼음이 용융에 의해 동위원소변화가 어떻게 발생하는가를 이해하는 것은 중요하며 등질성에 대한 연구는 수행되어 왔으나 이질성에 대한 연구는 거의 수행된 것이 없다. 본 연구에서는 모델연구 및 기존 실험연구를 이용하여 이질성의 스노우팩에서 물동위원소의 변동을 연구하였다. 본 연구는 Journal of Hydrology에 현재 투고중이다.

Snowmelt is an important component in the hydrological cycle and water management, and is under the influence of changing climate and meteorological events. In recent decades, a declining trend has been reported in snow cover, glaciers, and permafrost in many regions due to climate change (Hock et al., 2019), particularly, more significant for small glaciers such as European Alps (IPCC, 2019). Changing snow and glaciers further affects the amount and seasonality of runoff in snow-covered and glacier-fed basins, and induces challenges to water sources and agriculture (IPCC, 2019; Pan et al., 2018). In this context, water isotopes have been commonly used as tracers for hydrometeorological studies. Hence, it is necessary to better understand the isotopic evolution of snowmelt during the ablation period which further improve the quantification of hydrographic separation. Therefore, the present study examines the temporal changes in the isotopic composition of meltwater from a snowpack with isotopically distinct layers caused by meteorological conditions.

A one-dimensional model is used to simulate the isotopic variations of the meltwater by varying the initial isotopic compositions of the snow layers and parameters such as the effectiveness of exchange (ψ), the ice-to-liquid ratio of the exchange system (f), and the water saturation (S).

Modelling and experimental parameters have been shown in table 7.1 and 7.2. The isotopic evolution for both homogeneous and heterogeneous snow layers are shown in figure 7.1. Experimental data was modelled in the figure 7.2. The parameter sensitivities are represented in the figure 7.3 and 7.4. Based on the modelled data on sensitivity analysis, the slopes of δD vs. $\delta^{18}O$ were shown in table 7.3. This study also summarizes the isotopic variation in meltwater and its contribution to runoff reported in field observations.

The isotopic evolution is shown to be sensitive to the initial layering of enriched or depleted snow in the snowpack, and to the extent of isotopic difference of the layers. In addition, more distinct patterns are observed in the isotopic evolution as the ψ and f values are increased; particularly, a significant modification is observed in the bottom layer that is altered by the enriched top layer, thereby further affecting the pattern of isotopic evolution. The isotopic heterogeneity is suggested as a significant factor in the isotopic evolution of meltwater, even, various other influencing factors are considered in under natural conditions. Due to the close dependence of snow and glacial upon climate change, the present study is expected to support for further hydrometeorological studies particularly in snow-dominated regions.



Table 3.7.1. The model parameters used in the present simulation

| Parameter | Value | Source |
|---|-------------------------|-----------------------|
| Gravitational acceleration (g), m s^{-2} | 9.8 | – |
| Viscosity (μ), N s m^{-2} | 1.793 | Kestin et al., 1978 |
| Intrinsic permeability (k), m^{-2} | 2.2×10^{-9} | Colbeck, 1982 |
| Density of ice, g cm^{-3} | 0.917 | – |
| Density of water, g cm^{-3} | 1.000 | – |
| R (D/H) _{VSMOW} | 1.5576×10^{-4} | Hagemann et al., 1970 |
| R (¹⁸ O/ ¹⁶ O) _{VSMOW} | 2.0052×10^{-3} | Baertschi, 1976 |
| Equilibrium fractionation factor (α) for hydrogen | 1.0195 | O'Neil, 1968 |
| Equilibrium fractionation factor (α) for oxygen | 1.0031 | O'Neil, 1968 |
| Water saturation (S) | 0.06 | Taylor et al., 2002 |
| Porosity (ϕ), % | 0.57 | Taylor et al., 2002 |
| Irreducible water content (S _i) | 0.04 | Jordan, 1991 |
| Fraction of ice involved in isotopic exchange (f) | 0.3 | Taylor et al., 2002 |
| Dimensionless rate constant of isotopic exchange (Ψ) | 3.0 | Taylor et al., 2002 |
| Initial δD for the two layers, ‰ | –87.7 and –114.9 | Lee et al., 2010 |
| Initial $\delta^{18}\text{O}$ for the two layers, ‰ | –12.6 and –16 | Lee et al., 2010 |

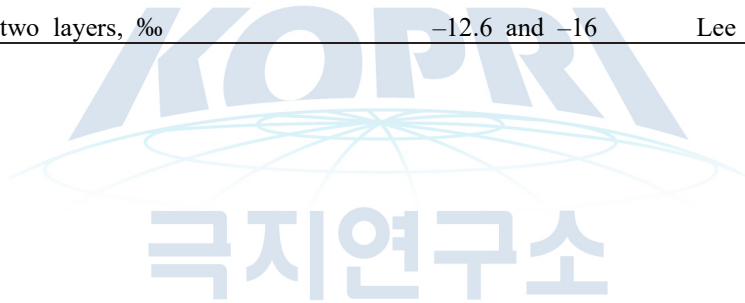


Table 3.7.2. The calculated and experimental values obtained from Herrmann et al. (1981) and Taylor et al. (2002).

| Parameter | Value | Source |
|--|--------|-----------------------|
| Bulk density (average of two layers), g cm^{-3} | 0.397 | Herrmann et al., 1981 |
| Snowpack height, cm | 35 | Herrmann et al., 1981 |
| Specific discharge, cm h^{-1} | 0.2 | Herrmann et al., 1981 |
| Porosity | 0.58 | Calculated |
| Percolation velocity, cm h^{-1} | 3.53 | Calculated |
| Water saturation (S) | 0.06 | Taylor et al., 2002 |
| Initial δD (top layer), ‰ | -141.4 | Herrmann et al., 1981 |
| Initial δD (bottom layer), ‰ | -124.8 | Herrmann et al., 1981 |
| Mass of liquid (a), g cm^{-3} | 0.06 | Calculated |
| Mass of ice (b), g cm^{-3} | 0.50 | Calculated |
| f | 0.3 | Optimized |
| ψ | 3 | Optimized |
| k_r , h^{-1} | 0.30 | Calculated |
| γ | 0.73 | Calculated |

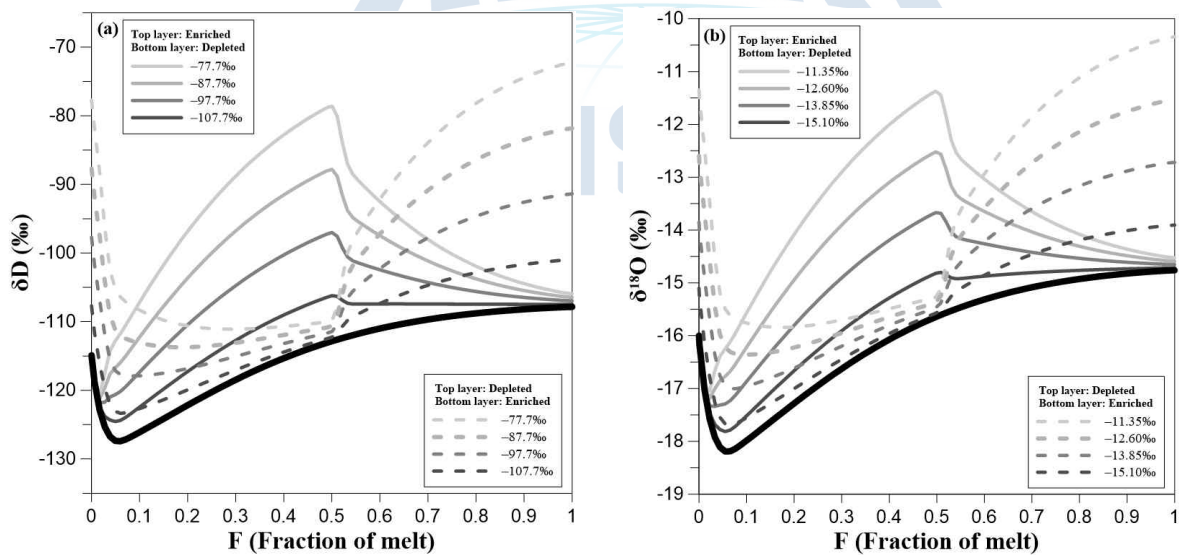


Fig 3.7.1. The modelled isotopic evolution of the meltwater by varying the isotopic difference between two layers: (a) δD ; (b) $\delta^{18}\text{O}$. The thick black lines represent the homogeneous layer with δD (-114.9‰) or $\delta^{18}\text{O}$ (-16‰); the thin lines are the simulations for an enriched top layer and depleted bottom layer, and the dashed lines are the simulations for a depleted top layer and enriched bottom layer.

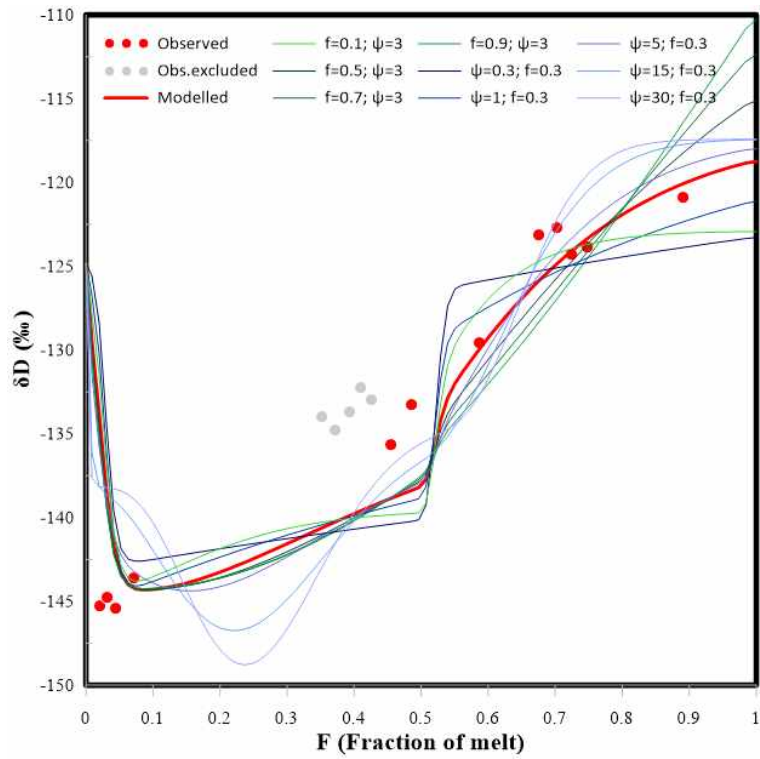


Fig 3.7.2. A comparison of the present model results (solid lines) with the experimental isotopic composition of meltwater according to Herrmann et al., 1981 (red circles). The red line is the good fit to the observed data. The grey circles represent outlying experimental data points that were excluded from the model fitting.



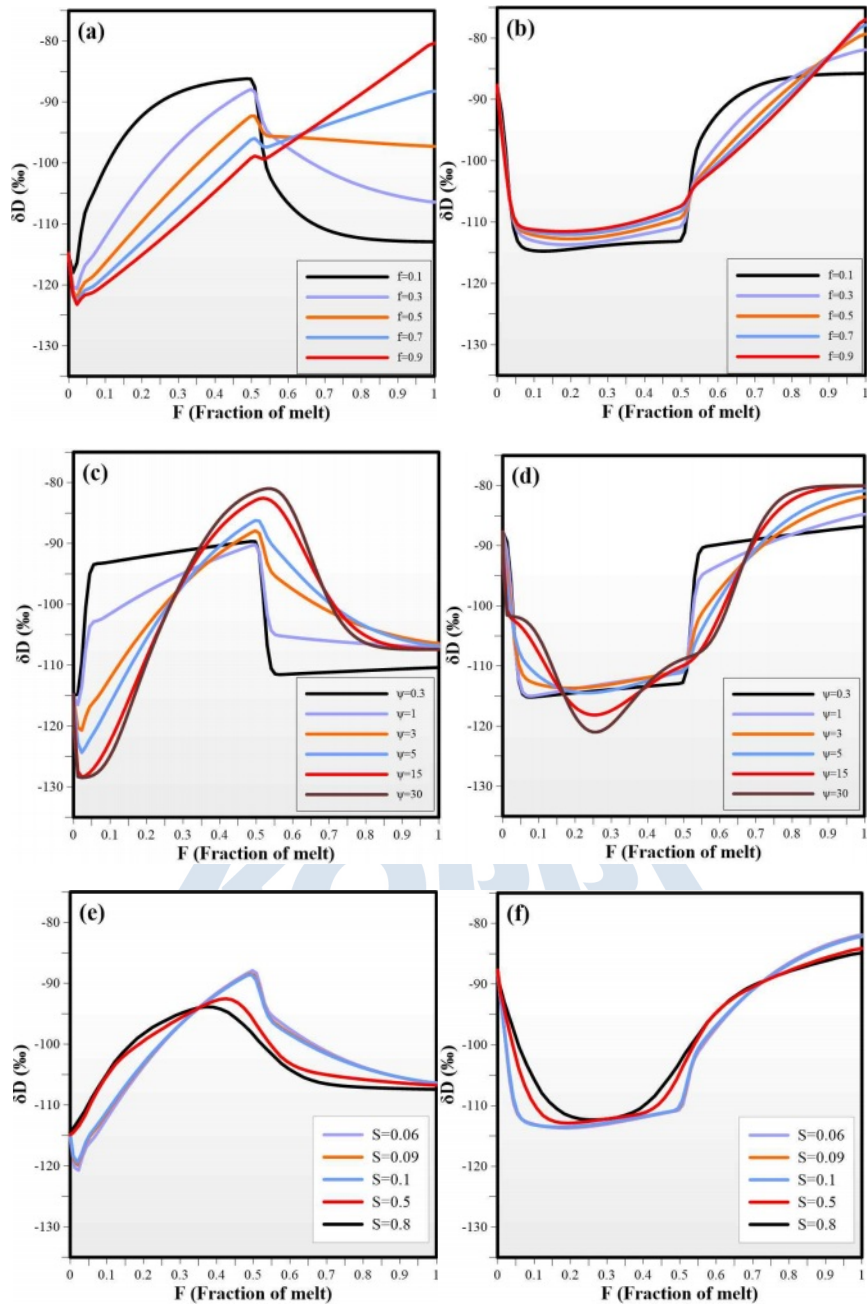


Fig 3.7.3. The simulated evolution of the δD value of meltwater as a function of the fraction (F) of melted snowpack with various values of f (a and b), ψ (c and d), and S (e and f), where the left-hand panels (a, c, and e) represent the results for the isotopically-depleted top layers and enriched bottom layers, while the right-hand panels (b, d, and f) represent the results for the isotopically-enriched top layers and depleted bottom layers.

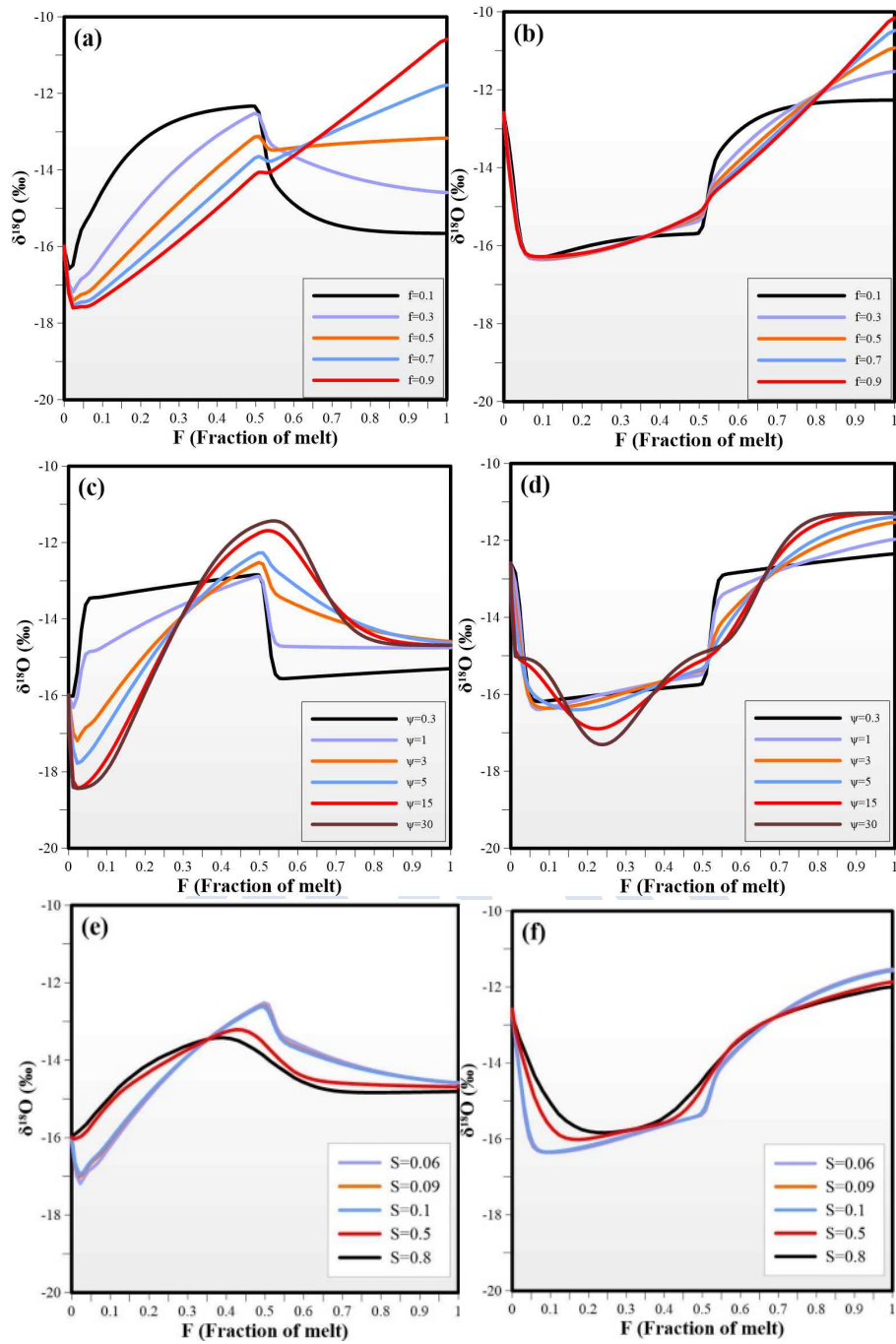


Fig 3.7.4. The simulated evolution of the $\delta^{18}\text{O}$ value of meltwater as a function of the fraction (F) of melted snowpack with various values of f (a and b), ψ (c and d), and S (e and f), where the left-hand panels (a, c, and e) represent the results for the isotopically-depleted top layers and enriched bottom layers, while the right-hand panels (b, d, and f) represent the results for the isotopically-enriched top layers and depleted bottom layers.

Table 3.7.3. The slopes of δD vs. $\delta^{18}O$ with various f , ϕ , and S values (Dep = depleted, Enr = enriched).

| Layer sequence | f = 0.1 | f = 0.3 | f = 0.5 | f = 0.7 | f = 0.9 | |
|-----------------------|--------------------------------|------------------------------|------------------------------|------------------------------|-------------------------------|-------------------------------|
| Dep-Enr | 6.85 | 7.60 | 6.37 | 6.04 | 5.81 | |
| Enr-Dep | 6.87 | 7.97 | 6.07 | 5.98 | 6.03 | |
| Layer sequence | $\Psi = 0.3$ | $\Psi = 1$ | $\Psi = 3$ | $\Psi = 5$ | $\Psi = 15$ | $\Psi = 30$ |
| Dep-Enr | 6.85 | 7.66 | 7.20 | 6.79 | 6.80 | 6.82 |
| Enr-Dep | 6.87 | 8.37 | 8.26 | 6.77 | 6.79 | 6.82 |
| Layer sequence | S = 0.06 | S = 0.09 | S = 0.1 | S = 0.5 | S = 0.8 | |
| Dep-Enr | 6.85 | 6.90 | 6.92 | 7.35 | 7.52 | |
| Enr-Dep | 6.87 | 6.99 | 7.03 | 7.92 | 8.05 | |



Table 3.7.4. The isotopic variation in meltwater and its contribution to runoff reported in some studies

| Location | Sample type | $\delta^{18}\text{O}$ and/or δD | Contribution to runoff | Melting season and study period | Reference |
|---|--|--|--|--------------------------------------|-------------------------|
| Permafrost catchment, Wolf Creek Research Basin, Yukon, Canada | Snowmelt | $\delta^{18}\text{O} = -25.9\text{‰}$ to -23.8‰ | ~21% of total freshet | April to June 2002 | Carey & Quinton, 2005 |
| Granger Basin within Wolf Creek Research basin, Canada | Snowmelt | $\delta^{18}\text{O} = -24.18\text{‰}$; $\delta\text{D} = -188.12\text{‰}$ | 32% based on $\delta^{18}\text{O}$; 23% based on δD | April to July 2008 | Boucher and Carey, 2010 |
| Western Mongolia (Upper Khovd River Basin) | Glacier melt | – | 15.4–18.7% (2000–2016) | Late June and early July | Pan et al., 2019 |
| Changbai Mountain area, semi-arid region in China | Snowmelt | $\delta^{18}\text{O} = -18.83\text{‰}$ to 12.38‰ ; $\delta\text{D} = -134.5\text{‰}$ to -85.34‰ | 14.4% to 59.8% | April to June, 2020 | Feng et al., 2022 |
| Juncal river basin, Central Chile | Glacier meltwater | $\delta^{18}\text{O} = -18.3\text{‰}$ to -17.1‰ ; $\delta\text{D} = -136.0\text{‰}$ to -126.8‰ | 50% to 90 % | 2011 to 2012 (unusual dry year) | Ohlanders et al., 2013 |
| High and Mid Atlas Mountain region, Morocco | Snow | $\delta^{18}\text{O} = -10.0\text{‰}$ to -2.4‰ ; $\delta\text{D} = -72.6\text{‰}$ to -11.6‰ | 47% | – | Rhoujjati et al., 2021 |
| Snowy range watershed in Southern Rocky Mountains, China | Snowmelt (event) | $\delta^{18}\text{O} = -18.27 \pm 0.52\text{‰}$ | 70.5% to 74.4% during melting event | Melting out by June | Millet et al., 2021 |
| Upper Ganga River near snout of the Gangotri Glacier, India | Snowmelt and glacial melt | Snowmelt: $\delta^{18}\text{O} = -14\text{‰}$ to -4‰ (mean = -11.4‰); $\delta\text{D} = -103\text{‰}$ to -27‰ (mean = -78.2‰) Glacial melt: $\delta^{18}\text{O} = -18.5\text{‰}$; $\delta\text{D} = -132.8\text{‰}$ | Snowmelt: 59.6% ; Glacial melt: 36.8% | During ablation period, 2004 to 2005 | Rai et al., 2019 |
| Forested (disturbed and undisturbed) mountain catchment, Šumava National Park, Czech Republic | Precipitation (Snow and rain) in the cold season | $\delta^{18}\text{O} = -14.1\text{‰}$ to -8.1‰ ; $\delta\text{D} = -100.3\text{‰}$ to -54.0‰ | $\delta^{18}\text{O} = 29\%$ to 65% ; $\delta\text{D} = 38\%$ to 53% | May to October | Vystavna et al., 2018 |
| Himalayan River (Satluj), India | Glacial, snow melt | $\delta^{18}\text{O} = -9.6\text{‰}$ to -24.7‰ | 15–64% | – | Maurya et al., 2018 |
| Beas basin, western Himalaya, India | Snow/Glacial melt | $\delta^{18}\text{O} = -10.05\text{‰}$ | 50% to annual runoff | April to June, 2010–2011 | Ahluwalia et al., 2013 |
| High elevation catchment of Rofenache stream, Alps | Snowmelt | $\delta^{18}\text{O} = -18.8\text{‰}$ (early melt event) to -17.9‰ (peak melt event) | 35% (early melt season) to 75% (peak season) | April to June 2014 | Schmieder et al., 2016 |
| Bridge Creek catchment in Italian Dolomites | Snow/Glacial melt | $\delta\text{D} = -26.1$ to -202.0‰ | 58–72% | March April 2011 to 2013 | Penna et al., 2016 |
| Tizinafu glacier river in north Kunlun Mountains, China | Ice meltwater | – | 28.31–65.43% | 2011–2012 | Fan et al., 2015 |
| Saldura river catchment in the Eastern Italian Alps | Snowmelt and glacial melt | Snowmelt: $\delta^{18}\text{O} = -15.62\text{‰}$ to -14.09‰ Glacial melt: $\delta^{18}\text{O} = -15.33\text{‰}$ to -13.86‰ | Snowmelt: 33% Glacial melt: 65% | May to July 2011–2013 | Engel et al., 2016 |
| Wind River Range watershed, American Rockies | Glacial melt | – | 53–59% | 2007–2008 | Cable et al., 2011 |

**Isotopic evolution of snowmelt and its hydrometeorological
importance in snow-covered regions**

By

Yalalt Nyamgerel ^a, Yeongcheol Han^b, Jeonghoon Lee ^{a, *}

^aDepartment of Science Education, Ewha Womans University, Seoul 120-750, Korea

^bDivision of Glacial Environment, Korea Polar Research Institute, Incheon 21990, Korea



제 4 장 연구개발목표 달성도 및 대외기여도

연구기간 3년동안 목표였던 해외논문 5편 국내논문 1편은 현재 출판된 해외논문 3편, 투고된 논문 2편, 출판된 국내논문 3편으로 목표는 달성한 것으로 판단된다. 또한 해외논문 1편을 준비 중에 있기 때문에 연구제안시 목표하였던 내용은 거의 다 근접한 것으로 판단된다. 또한, 국내외 학회에서 연구내용을 발표하여 본 과제를 홍보한 것으로도 판단된다. 아래 표에 이러한 내용을 정리하여 제시하였다.



| 성과목표 | 세부목표 | | 달성 주요내용 | 달성도(%) |
|-------------------------------------|------|-------------------------------------|---|---|
| 1. 빙하코어시료의 안정동위원소분석 및 기후인자와의 상관성 분석 | 1-1 | 빙하코어시료의 안정동위원소분석 및 미량원소분석 | - 스틱스지역의 편(firn) 코어의 불안정동위원소분석을 완료하였으며, 현재 미량원소분석을 수행하고 있음 | - 논문출판(Nyamgerel et al., 2020, Journal of Glaciology) |
| | 1-2 | 분석된 안정동위원소를 이용하여 빙하의 연대측정 | - 스틱스빙하시료의 안정동위원소 및 주요이온, 모델결과를 활용하여 25년의 연대를 추정하였음 | |
| | 1-3 | 빙하의 연대측정을 통한 강설량 복원 | - 빙하의 연대측정을 통한 스틱스지역의 강설량을 추정하여 해빙과의 상관관계를 밝혔음 | |
| 2. 기후인자와 대기대순환과의 상관성분석 | 2-1 | 복원된 강설량과 기후인자와의 상관성 파악 | - 스노우핏 시료를 이용하여 해빙의 면적과 안정동위원소 값에 상관성이 있음을 밝혔음 - ¹⁷ O의 빙하연구 가능성에 대하여 타진하였음 | - 논문출판(Nyamgerel et al., 2021, Earth Interactions) - 논문출판(Hur et al., 2021, Polish Polar Research) |
| | 2-2 | 기후인자와 대기대순환과의 상관성 연구 | - 스노우핏을 이용하여 월평균안정동위원소 값이 대기온도와 상관관계가 있음을 밝혔음 | |
| 3. 빙하코어시료를 이용한 과거 대기대순환 복원 | 3-1 | 빙하코어시료와 대기대순환과의 상관성을 설명할 수 있는 프록시개발 | - 빙하코어의 미량원소분석 결과를 향후 기상자료와 비교하기 위하여 스틱스지역에서 가져온 편코어의 미량원소 분석결과 분석 및 정리. - 빙하코어의 melting layer 해석하기 위해 얼음 용해 실험 수행하였음. | -논문투고(Nyamgerel et al., submitted, Journal of Hydrology) |
| | 3-2 | 빙하코어시료로부터 과거대기대순환 복원 | - 자료 분석 및 정리 | -논문투고예정(Nyamgerel et al., in prep, Journal of Geophysical Research – Atmosphere) |

제 5 장 연구개발결과의 활용계획

본 연구는 단기적으로 빅토리아 지역에서 시추된 빙하코어의 화학성분과 동위원소성분을 분석하여 짧은 기간의 기상변수와 긴 기후변수와의 상관관계를 찾는 것이 연구목표이다. 분석된 화학성분과 동위원소성분이 단계 1(level 1)의 자료라면, 연대측정을 통해 추정된 강설량은 단계 2(level 2) 자료라고 볼 수 있다. 강설량은 주변 해빙면적, 대기대순환과 밀접한 연관성이 있어 강설량과 이러한 변수간의 상관성을 파악한다면 과거의 강설량을 추정하고 이로부터 기상인자를 유도해 낼 수 있을 것으로 기대된다. 강설량은 미량원소의 농도에 영향을 끼치기 때문에 미량원소와 기상변수간의 상관성을 파악하는 것이 중요하다. 따라서, 스틱스 지역에서 시추한 빙하코어시료의 미량원소를 분석 중에 있으며, 이를 활용하는 것은 매우 중요할 것으로 판단된다. 미량원소 시료처리과정 및 분석에 대하여 다음과 같이 요약하였다.

Styx ice core sections were decontaminated before the trace element analysis. Because of the low concentration levels of trace elements in Antarctic snow and the vulnerability to contamination, mechanical decontamination procedure is required before analysis (Hong et al., 2003). The internal part of the ice cores considered to be less contaminated and restored the true concentration (Han et al., 2020). The ice core section between the depth of 4.32 to 9.87 m were manually decontaminated by removing the outer ~ 1 cm layer using cleaned ceramic knives (Kyocera, Japan). Decontamination procedure was followed an ultraclean procedure (Han et al., 2020). Density of the ice core section was ranged between 460 to 510 kg/m³. Average length of the ice core sections was 0.43 m, and the ice core sections were cut into appropriate subsections to be held in plastic holder during decontamination. Dimension of the ice core sections were 3.5 × 4.25 cm cross section, average 15.5 cm in length for the ice core depth between 4.32 m to 7.07 m. For the depth between 7.17 m to 9.87 m, the ice cores dimensions were 5.8 × 5.8 cm cross section, average 21.3 cm in length. Sample cutting resolution was averagely 5.5±1 cm. Cutting resolution was varied depending on the conditions of the ice core section.

Decontamination, sample preparation, and analytical procedures were performed in the clean facilities at KOPRI. All utensils used in the sample preparation was pre-cleaned and this procedure was successfully used for trace element analysis in ice (Han et al., 2020). All analytical instruments were placed within a Class 10 laminar flow clean booth inside a Class 1000 clean room at KOPRI. Ultrapure water (18.2M Ω -cm resistivity) produced by a Millipore RO water purifier (Model Elix-3) with a Milli-Q system (Milli-Q Academic, Millipore Corp, Darmstadt, German) was used in various steps in cleaning procedures. Sub-boiling ultra-pure water (DuoPUR, Milestone, Sorisole, Italy) was used for preparation of blank and standard solutions.

The ice core samples were melted at room temperature in the LDPE bottles (500 ml or 1000 ml bottle) inside the Class 10 clean bench. After melting, the samples were acidified to 1% using ultrapure HNO₃⁻ (Fisher Optima grade nitric acid). Concentrations of trace elements in total 81 samples were analyzed by Inductively coupled plasma-sector field spectrometry (ICP-SF-MS, Element2, Thermo Fischer Scientific, Germany) equipped with Apex high-sensitivity inlet system (Apex IR, Elemental

Scientific Incorporated Omaha, Nebraska, US) at KOPRI.

Multi standard calibration was used and Rh was used as an internal standard. A certified reference material SLRS-6 (Certified Riverine Water Reference Material by National Research Council, Ottawa, ON, Canada) were diluted and analyzed for analytical accuracy. The analysis on SLRS6 show a good recovery within 19% except fo Sb, Tl, Th, U, Al, and Cr. Detection limits were calculated by three times the standard deviation of eight blank samples (Tables 8.1 and 8.2). REEs and Rb, Sr, Mo, Cd, Sb, Ba, Tl, Pb, Bi, Th, and U were analyzed in low resolution mode. While Al, Sc, Ti, V, Ce, Mn, Fe, Co, Ni, Cu, and Zn were measured in mid resolution mode. As was only measured in high resolution mode.

To test the decontamination procedure. Three outside layers were collected, and the outermost layer was compared to the 2nd layer (middle). We note that the amount the third layer was very low thus the concentration was not able to be compared with outer layer. Trace elements concentration in the middle layer was lower by 1.03 (Ln) to 73.83 (Cr) times than those in the outermost layer in the depth corresponding to 4.73 m to 4.97 m. For the depth interval between 7.17 m to 7.57 m, the concentration decreases by 1.50 (Rb) and 147.54 (Cd) times. The middle layer in 7.82 m to 8.24 m also show the concentrations 1.51 (Rb) to 32.67 (Bi) times lower than the outermost layer. While the U and Mn show slightly high concentration (0.17 and 0.12 times high) in the middle layer corresponding the depth ranges between 6.63 and 6.76 m. Also, at the depth of 7.67 to 7.73 m, some elements (Th, U, Al, Ti, Fe) increasing concentration in the middle layer. Although it is usually accepted the lower concentration in inner layers than outermost layer, we state that there can variation randomly due to the mechanical handling (chiseling length may differ). Moreover, the inner sample corresponding to the 7.67 m depth had high concentration, thus it can be expected that more chisels from this depth collected in middle layers. Age dating for the depths corresponding to the trace elemens samples were interpolated based on the age scale estimated by water isotopes and ions.

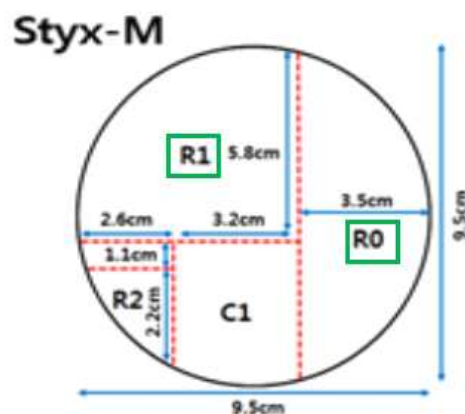


Fig 5.1. R1 and R0 (half of it) section that used for trace element analysis

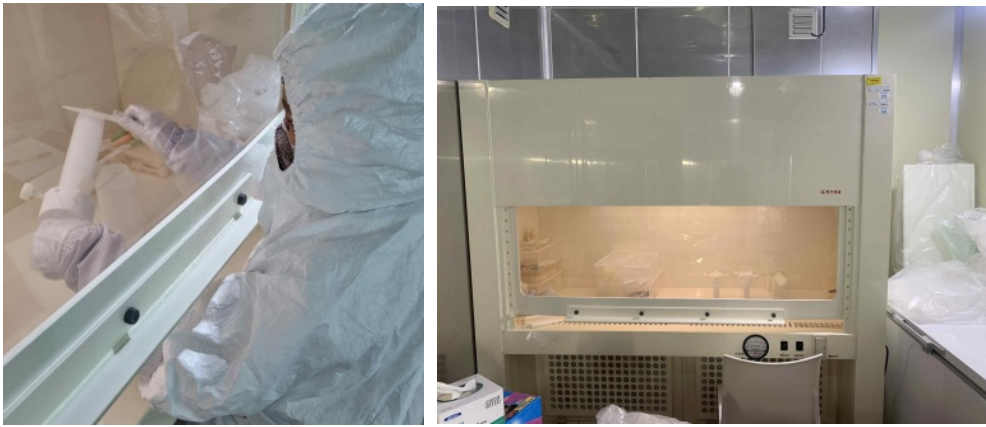


Fig 5.2. Chiselling procedure of the portions of Styx-M ice core for trace elements analysis and the class 100 clean bench in a cold room at KOPRI.



Fig 5.3. Inner layer with diameter of ~1-1.2 cm after chiselling for the depth sections between 4.2 to 6.2m



Fig 5.4. Inner layer with diameter of ~3 cm after chiselling for the depth sections between 6.2 to 9.8m

Table 5.1. Mean, standard deviation (SD), median, max, min, and DL in pg g^{-1} of trace elements

| | Element | Mean | SD | Max | Min | Range | n | DL |
|---|----------------|-------------|-----------|------------|------------|--------------|----------|-----------|
| 1 | Rb | 15.37 | 19.92 | 94.81 | 0.99 | 95.64 | 81 | 0.010 |
| 2 | Sr | 286.90 | 677.62 | 3609.80 | 1.80 | 2002.92 | 81 | 0.042 |

| | | | | | | | | |
|----|----|---------|---------|----------|-------|---------|----|-------|
| 3 | Mo | 4.04 | 15.55 | 129.90 | 0.07 | 1960.17 | 81 | 0.030 |
| 4 | Cd | 2.48 | 2.32 | 14.12 | 0.51 | 27.77 | 81 | 0.018 |
| 5 | Sb | 0.43 | 0.68 | 4.75 | 0.05 | 89.77 | 81 | 0.024 |
| 6 | Ba | 38.58 | 56.40 | 382.17 | 2.65 | 144.01 | 81 | 0.063 |
| 7 | Tl | 2.09 | 17.09 | 153.97 | 0.02 | 7810.11 | 81 | 0.009 |
| 8 | Pb | 52.41 | 120.07 | 901.22 | 1.85 | 487.32 | 81 | 0.342 |
| 9 | Bi | 0.08 | 0.08 | 0.43 | 0.01 | 55.48 | 75 | 0.005 |
| 10 | Th | 1.05 | 1.99 | 14.06 | 0.02 | 872.94 | 81 | 0.001 |
| 11 | U | 0.28 | 0.49 | 2.71 | 0.00 | 828.42 | 80 | 0.003 |
| 12 | Al | 3246.28 | 7777.26 | 60846.28 | 7.30 | 8330.47 | 80 | 0.755 |
| 13 | Ti | 261.15 | 475.95 | 2586.57 | 0.49 | 5273.71 | 81 | 0.148 |
| 14 | V | 6.39 | 10.12 | 46.59 | 0.01 | 4689.26 | 78 | 0.013 |
| 15 | Cr | 10.25 | 33.63 | 262.41 | 0.14 | 1839.56 | 62 | 0.073 |
| 16 | Mn | 125.39 | 212.02 | 1534.14 | 1.02 | 1503.91 | 81 | 0.020 |
| 17 | Fe | 2757.99 | 4950.40 | 30529.82 | 3.14 | 9730.39 | 81 | 0.861 |
| 18 | Co | 5.06 | 9.61 | 78.81 | 0.06 | 1378.03 | 81 | 0.014 |
| 19 | Ni | 1139.35 | 2723.20 | 15699.84 | 3.96 | 3963.45 | 81 | 0.522 |
| 20 | Cu | 164.07 | 505.95 | 4156.93 | 1.12 | 3700.62 | 81 | 0.194 |
| 21 | Zn | 1336.42 | 1161.55 | 6088.50 | 23.38 | 260.36 | 81 | 1.101 |
| 22 | As | 4.98 | 3.89 | 29.89 | 0.78 | 38.33 | 73 | 0.322 |

Table 5.2. Mean, SD, median, max, min, and DL in $\mu\text{g g}^{-1}$ of rare earth elements

| | Element | Mean | SD | Max | Min | Range | n | DL |
|----|----------------|-------------|-----------|------------|------------|--------------|----------|-----------|
| 1 | Sc | 0.69 | 1.01 | 5.52 | 0.03 | 218.29 | 64 | 0.024 |
| 2 | La | 3.98 | 8.16 | 53.40 | 0.03 | 1861.90 | 81 | 0.002 |
| 3 | Ce | 8.59 | 18.63 | 104.65 | 0.06 | 1614.49 | 81 | 0.003 |
| 4 | Pr | 0.87 | 1.79 | 11.53 | 0.01 | 1972.20 | 81 | 0.002 |
| 5 | Nd | 3.37 | 7.26 | 47.34 | 0.03 | 1585.25 | 80 | 0.037 |
| 6 | Sm | 0.58 | 1.25 | 7.17 | 0.01 | 1095.65 | 81 | 0.005 |
| 7 | Eu | 0.13 | 0.31 | 2.03 | 0.00 | 468.47 | 75 | 0.004 |
| 8 | Gd | 0.54 | 1.14 | 6.56 | 0.01 | 487.95 | 75 | 0.012 |
| 9 | Tb | 0.07 | 0.15 | 0.89 | 0.00 | 635.25 | 76 | 0.001 |
| 10 | Dy | 0.39 | 0.86 | 5.06 | 0.01 | 818.32 | 78 | 0.003 |
| 11 | Ho | 0.07 | 0.14 | 0.88 | 0.00 | 458.44 | 79 | 0.001 |
| 12 | Er | 0.17 | 0.36 | 2.26 | 0.00 | 1026.70 | 81 | 0.001 |
| 13 | Yb | 0.17 | 0.31 | 1.91 | 0.00 | 715.46 | 65 | 0.006 |
| 14 | Lu | 0.02 | 0.04 | 0.26 | 0.00 | 224.28 | 75 | 0.001 |

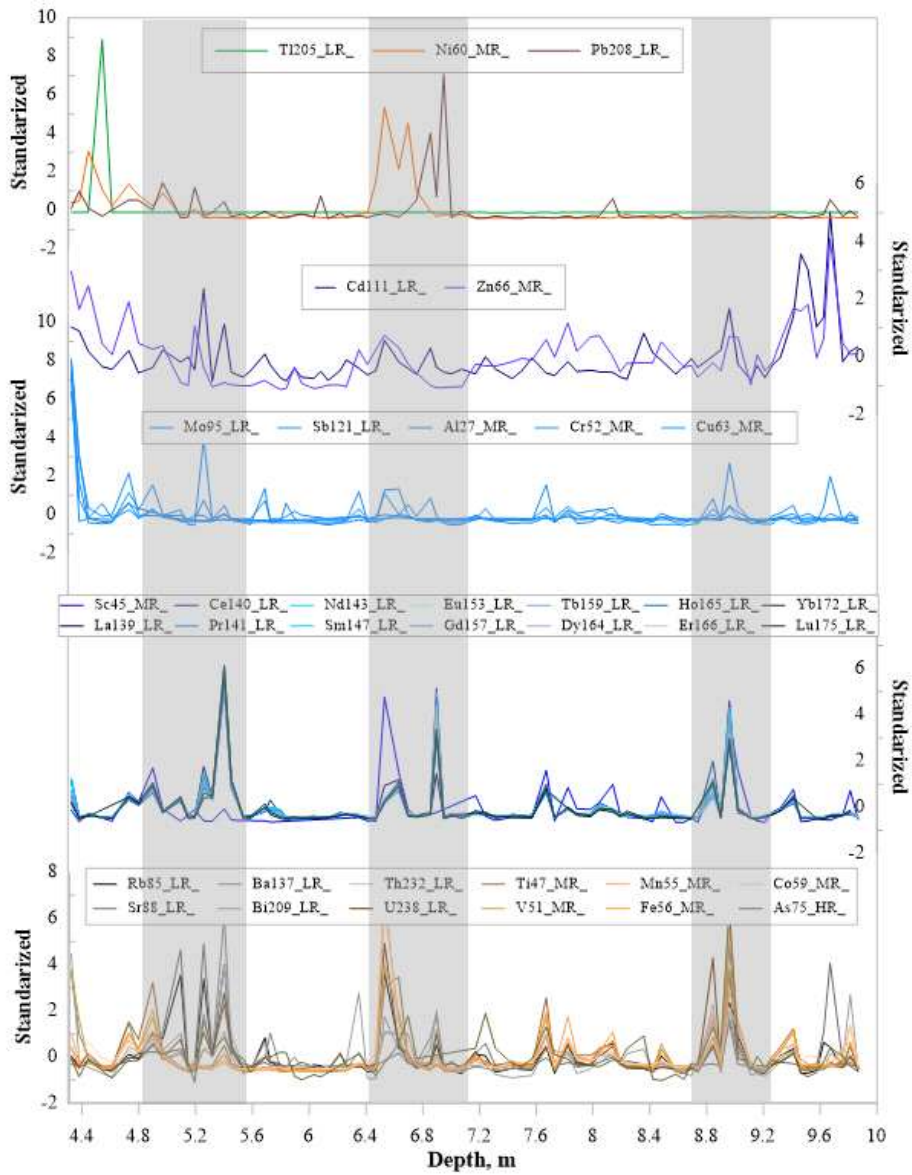


Fig 5.5. Depth vs standardized profile of trace elements measured in the portion of Styx-M ice core

제 6 장 연구개발과정에서 수집한 해외과학기술정보

연구개발과정에서 수집한 다양한 과학기술정보는 두 편의 리뷰논문을 출판하였다. Nyamgerel et al. (2021, molecules)에서는 17O를 분석하고 이를 남극 빙하코어시료에 어떻게 적용할 수 있을지에 대한 해외 사례 및 국내 적용가능성에 대하여 논하였다. 또한, 이정훈 외(2021, 한국 지구과학회지)에서는 희토류원소의 빙하연구 활용에 대하여 논의하였다. 이는 3장에 자세하게 설명되어 있다.



제 7장 참고문헌

1. Affolter, S and 4 others (2015) Triple isotope (δD , $\delta^{17}O$, $\delta^{18}O$) study on precipitation, drip water and speleothem fluid inclusions for a Western Central European cave (NW Switzerland). *Quat. Sci. Rev.* 2015, 127, 73 - 89.
2. Aron, P.G and 8 others (2004) Triple oxygen isotopes in the water cycle. *Chem. Geol.* 2020, 565, 120026.
3. Becagli, S and 12 others (2004) Chemical and isotopic snow variability in East Antarctica along the 2001/02 ITASE traverse. *Annals of Glaciology*, 39, 473-482. doi:10.3189/172756404781814636.
4. Bertler, N. A. N and 5 others (2004) El Niño suppresses Antarctic warming. *Geophys. Res. Lett.*, 31, L15207, doi:10.1029/2004GL020749.
5. Caiazza L and 25 others (2017) Prominent features in isotopic, chemical and dust stratigraphies from coastal East Antarctic ice sheet (Eastern Wilkes Land). *Chemosphere.*, 176, 273-287.
6. Dansgaard W (1964) Stable isotopes in precipitation. *Tellus.*, 16(4), 436-468, (doi: 10.3402/tellusa.v16i4.8993).
7. Dee DP and 35 others (2011) The ERA Interim reanalysis: configuration and performance of the data assimilation system. *Q.J.R. Meteorol. Soc.*, 137 (656), 553-597.
8. Dinniman, M.S and 2 others (2012) Sensitivity of Circumpolar Deep-Water Transport and Ice Shelf Basal Melt along the West Antarctic Peninsula to Changes in the Winds. *Journal of Climate*, 2012. 25(14): p. 4799-4816.
9. Frezzotti M and 13 others (2004) "New estimations of precipitation and surface sublimation in East Antarctica from snow accumulation measurements. *Climate Dynamics.*, 23, 803-813.
10. Furukawa R and 6 others (2017) Seasonal scale dating of a shallow ice core from Greenland using oxygen isotope matching between data and simulation. *Journal of Geophysical Research: Atmospheres.*, 122, 10873 - 10887, (doi.org/10.1002/2017JD026716).
11. Gragnani, R and 3 others (1998) Chemical and isotopic profiles from snow pits and shallow firn cores on Campbell Glacier, northern Victoria Land, Antarctica. *Annals of Glaciology.*, 27, 679-684, https://doi.org/10.3198/1998AoG27-1-679-684.
12. Han YC and 7 others (2015) Shallow ice-core drilling on Styx glacier, northern Victoria Land, Antarctica in the 2014-2015 summer. *Journal of the Geological Society of Korea.*, 51(3), 343-355.
13. Hwang, H and 2 others (2021) "Distribution of Rare Earth Elements and Their Applications as Tracers for Groundwater Geochemistry - A Review," *Journal of the Korean earth science society*. The Korean Earth Science Society. doi: 10.5467/jkess.2021.42.4.383.
14. Hock, R and 12 others (2019). High mountain areas. Special report on the ocean and cryosphere in a changing climate: IPCC.
15. IPCC, 2019: Technical Summary [H.-O. Pörtner, D.C. Roberts, V. Masson-Delmotte, P. Zhai, E. Poloczanska, K. Mintenbeck, M. Tignor, A. Alegría, M. Nicolai, A. Okem, J. Petzold, B. Rama, N.M. Weyer (eds.)]. In: IPCC Special Report on the Ocean and Cryosphere in a Changing Climate [H.- O. Pörtner, D.C. Roberts, V. Masson-Delmotte, P. Zhai, M. Tignor, E. Poloczanska, K. Mintenbeck, A. Alegría, M. Nicolai, A. Okem, J. Petzold, B. Rama, N.M. Weyer (eds.)]. In press.
16. Kwak H and 6 others (2015) A Study on High-Resolution Seasonal Variations of Major Ionic Species in Recent Snow Near the Antarctic Jang Bogo Station. *Ocean & Polar Research.*, 37 (2), 127-140, (doi: 10.4217/OPR.2015.37.2.127).
17. Landais, A and 2 others (2008) Record of $\delta^{18}O$ and $\delta^{17}O$ -excess in ice from Vostok Antarctica during the last 150,000 years. *Geophys. Res. Lett.* 2008, 35, 1 - 5.
18. Landais, A and 5 others (2012) Triple isotopic composition of oxygen in surface snow and water vapor at NEEM (Greenland). *Geochim. Cosmochim. Acta.* 2012, 77,

- 304 - 316.
19. Landais, A and 3 others (2012b) Seasonal variations of $\delta^{17}O$ -excess and δ^d -excess in snow precipitation at Vostok station, East Antarctica. *J. Glaciol.* 2012, 58, 725 - 733.
 20. Legrand M and Mayewski P (1997) Glaciochemistry of polar ice cores: A review. *Review of Geophysics.*, 35(3), 219 - 243, (doi: 10.1029/96RG03527).
 21. Li, S and 2 others (2015) Continental scale variation in $\delta^{17}O$ -excess of meteoric waters in the United States. *Geochim. Cosmochim. Acta* 2015, 164, 110 - 126.
 22. Li, S and 4 others (2017) Triple oxygen isotope composition of leaf waters in Mpala, central Kenya. *Earth Planet. Sci. Lett.* 2017, 468, 38 - 50.
 23. Luz, B and Barkan, E (2010). Variations of $\delta^{17}O/16O$ and $\delta^{18}O/16O$ in meteoric waters. *Geochim. Cosmochim. Acta* 2010, 74, 6276 - 6286.
 24. Pang, H and 9 others (2015) Spatial distribution of $\delta^{17}O$ -excess in surface snow along a traverse from Zhongshan station to Dome, East Antarctica. *Earth Planet. Sci.Lett.* 2015, 414, 126 - 133.
 25. Masson-Delmotte V and 35 others, (2008) A review of Antarctic surface snow isotopic composition: Observations, atmospheric circulation, and isotopic modeling. *Journal of Climate.*, 21, 3359-3387, (doi:10.1175/2007JCLI2139.1).
 26. Mouginit, J and 2 others (2013) Sustained increase in ice discharge from the Amundsen Sea Embayment, West Antarctica, from 1973 to 2013. *Geophysical Research Letters*, 2014: p. 2013GL059069.
 27. Mulvaney, R and 8 others (2021) Ice drilling on Skytrain Ice Rise and Sherman Island, Antarctica. *Annals of Glaciology*, 62(85-86), 311-323. doi:10.1017/aog.2021.7.
 28. Neff, P. 2020. Amundsen Sea coastal ice rises: Future sites for marine-focused ice core records. *Oceanography* 33-2:88 - 89, <https://doi.org/10.5670/oceanog.2020.215>.
 29. Nyamgerel, Y and 5 others (2020) Chronological characteristics for snow accumulation on Styx Glacier in northern Victoria Land, Antarctica. *Journal of Glaciology*, 1-11. Doi:10.1017/jog.2020.53.
 30. Nyamgerel, Y and 5 others (2021) Snow-pit record from a coastal Antarctic site and its preservation of meteorological features. *Earth Interact.* 25, 108 - 118. doi:10.1175/ei-d-20-0018.1.
 31. Nyamgerel, Y and 5 others (2021) Review on applications of $\delta^{17}O$ in hydrological cycle. *Molecules*, 26, 4468. <https://doi.org/10.3390/molecules26154468>.
 32. Pan, C. G and 5 others (2018). Glacier Recession in the Altai Mountains of Mongolia in 1990-2016. *Geografiska Annaler: Ser. A, Phys. Geogr.* 100, 185 - 203. doi:10.1080/04353676.2017.1407560.
 33. Passey, B.H and Ji, H (2019) Triple oxygen isotope signatures of evaporation in lake waters and carbonates: A case study from the western United States. *Earth Planet. Sci. Lett.* 2019, 518, 1 - 12.
 34. Schoenemann, S.W and 4 others (2014) Triple water-isotopologue record from WAIS Divide, Antarctica: Controls on glacial-interglacial changes in $\delta^{17}O$ -excess of precipitation. *J. Geophys. Res. Atmos.* 2014, 119, 8741 - 8763.
 35. Severi, M., S and 5 others (2009) Thirty years of snow deposition at Talos Dome (Northern Victoria Land, East Antarctica): Chemical profiles and climatic implications, *Microchem. J.*, 92, 15 - 20, 2009.
 36. Rhodes RH and 6 others (2012) Little Ice Age climate and oceanic conditions of the Ross Sea, Antarctica from a coastal ice core record. *Climate of the Past.*, 8, 1223 - 1238, (<https://doi.org/10.5194/cp-8-1223-2012>, 2012)
 37. Sinclair, K. E and 2 others (2010) Synoptic controls on precipitation pathways and snow delivery to high-accumulation ice core sites in the Ross Sea region, Antarctica, *J. Geophys. Res.*, 115, D22112, doi:10.1029/2010JD014383.
 38. Steig, E.J., and Neff P.D. 2018. The prescience of paleoclimatology and the future of the Antarctic ice sheet. *Nat Commun* 9, 2730 (2018). <https://doi.org/10.1038/s41467-018-05001-1>.
 39. Stenni B and 6 others (2000) Snow accumulation rates in northern Victoria Land, Antarctica, by firn-core analysis. *Journal of Glaciology.*, 46(155), 541 - 552.
 40. Stenni B and 18 others (2017) Antarctic climate variability on regional and

- continental scales over the last 2000 years. *Climate of the Past*, 13, 1609 - 1634, (<https://doi.org/10.5194/cp-13-1609-2017>).
41. Stenni B and 6 others (2002) Eight centuries of volcanic signal and climate change at Talos Dome (East Antarctica). *Journal of Geophysical Research*, 107(D9), 1-14, doi:10.1029/2000JD000317, 2002.
 42. Surma, J and 3 others (2015) Triple oxygen isotope signatures in evaporated water bodies from the Sistan Oasis, Iran. *Geophys. Res. Lett.* 2015, 42, 8456 - 8462
 43. Surma, J and 2 others (2021) Triple Oxygen Isotope Systematics in the Hydrologic Cycle. *Rev. mineral. Geochem.* 2021, 86, 401 - 428.
 44. Thomas, E. R and 15 others (2017) Regional Antarctic snow accumulation over the past 1000 years, *Clim. Past*, 13, 1491 - 1513, <https://doi.org/10.5194/cp-13-1491-2017>, 2017.
 45. Tian, C and Wang, L (2019) Data Descriptor: Stable isotope variations of daily precipitation from 2014 - 2018 in the central United States. *Nat. Publ. Gr.* 2019, 9, 1 - 8.
 46. Touzeau, A and 17 others Acquisition of isotopic composition for surface snow in East Antarctica and the links to climatic parameters. *Cryosphere* 2016, 10, 837 - 852.
 47. Traversi R and 6 others (2004) Spatial and temporal distribution of environmental markers from coastal to plateau areas in Antarctica by firn core chemical analysis. *International Journal of Environmental Analytical Chemistry*, 84(6 - 7), 457 - 470. (doi.org/10.1080/03067310310001640393).
 48. Tuohy A and 6 others (2015) Transport and deposition of heavy metals in the Ross Sea Region, Antarctica. *Journal of Geophysical Research: Atmosphere*, 120, 10,996 - 11,011, (doi:10.1002/2015JD023293).
 49. Udisti R (1996) Multiparametric approach for chemical dating of snow layers from Antarctica. *International Journal of Environmental Analytical Chemistry*, 63, 225-244.
 50. Uechi, Y and Uemura, R (2019) Dominant influence of the humidity in the moisture source region on the ^{17}O -excess in precipitation on a subtropical island. *Earth Planet. Sci. Lett.* 2019, 513, 20 - 28.
 51. Uemura, R and 3 others (2010) Triple isotope composition of oxygen in atmospheric water vapor. *Geophys. Res. Lett.* 2010, 37, 1 - 4.
 52. Winkler, R and 7 others (2012) Deglaciation records of ^{17}O -excess in East Antarctica: Reliable reconstruction of oceanic normalized relative humidity from coastal sites. *Clim. Past*. 2012,8, 1 - 16.
 53. Winkler, R and 9 others (2013). Interannual variation of water isotopologues at Vostok indicates a contribution from stratospheric water vapor. *Proc. Natl. Acad. Sci. USA* 2013, 110, 17674 - 17679.
 54. Yang J W and 10 others (2018) Surface temperature in twentieth century at the Styx Glacier, northern Victoria Land, Antarctica, from borehole thermometry. *Geophysical Research Letters*, 45, 9834-9842, (doi.org/10.1029/2018GL078770).

뒷 면

주 의

1. 이 보고서는 극지연구소 위탁과제 연구결과보고서입니다.
2. 이 보고서 내용을 발표할 때에는 반드시 극지연구소에서 위탁연구과제로 수행한 연구결과임을 밝혀야 합니다.
3. 국가과학기술 기밀유지에 필요한 내용은 대외적으로 발표 또는 공개하여서는 안됩니다.

위탁과제 국·영문 사사(acknowledgment) 표기 방법

국문 표기

- 이 연구는 극지연구소의 지원을 받아 수행되었습니다.(본과제 계정번호*)

* 본과제 계정번호: 극지연구소에서 부여한 과제번호로 연구소 연구관리담당부서에 확인

영문 표기

- This work was supported by the Korea Polar Research Institute (KOPRI, 본과제 계정번호)

* 연구결과의 발표 내용에 따라 위의 표기방식을 변경할 수 있으나, 밑줄 친 내용이 반드시 포함되어야 함

극지연구소